Journal of Materials Research and Technology 28 (2024) 911–934

Contents lists available at ScienceDirect

Journal of Materials Research and Technology

journal homepage: www.elsevier.com/locate/jmrt

# Review on wear resistance of laser cladding high-entropy alloy coatings

Dingding Xiang [a,b,c,d], Yusheng Liu [a], Tianbiao Yu [a], Di Wang [a], Xiaoxin Leng [a], Kaiming Wang [e], Lin Liu [f], Jie Pan [f], Sun Yao [a,*], Zibin Chen [d,**]

[a] School of Mechanical Engineering and Automation, Foshan Graduate School of Innovation, Northeastern University, Shenyang, 110819, China
[b] State Key Laboratory of Solid Lubrication, Lanzhou Institute of Chemical Physics, Chinese Academy of Science, Lanzhou, 730000, China
[c] Key Laboratory for Precision and Non-Traditional Machining Technology of Ministry of Education, Dalian University of Technology, Dalian, 116024, China
[d] State Key Laboratory of Ultra-precision Machining Technology, Research Institute for Advanced Manufacturing, Department of Industrial and Systems Engineering, The Hong Kong Polytechnic University, Hong Kong, 100872, China
[e] State Key Laboratory of Tribology in Advanced Equipment, Tsinghua University, Beijing, 100084, China
[f] School of Materials Science and Engineering, State Key Lab for Materials Processing and Die & Mold Technology, Huazhong University of Science and Technology, Wuhan, 430074, China

ARTICLE INFO

*Keywords:*
Laser cladding
High-entropy alloys
Wear resistance
A review
Coatings

ABSTRACT

The wear resistance of the part surface has become an important factor affecting its own service life. Laser cladding (LC), as a surface modification technology, can prepare a coating with good metallurgical bonding with the substrate, which can significantly improve the wear resistance of the material surface. High entropy alloys (HEAs) are an emerging coating material with excellent wear resistance. Therefore, this paper reviews the latest development status in wear resistance of laser cladding-high-entropy alloy coatings (LC-HEACs) in terms of the HEAs material system, LC process parameters, strengthening phase, amorphous phase strengthening, assisted cladding, and post-treatment. At the same time, this paper also expounds on the mechanism of LC-HEACs enhancing the surface wear resistance of materials, and the current research status of LC-HEACs in different engineering materials and application environments. Finally, the current research deficiencies, challenges, and future development trends of LC-HEACs in the field of wear resistance are also elaborated, and it is expected to provide some references for their future development and applications.

## 1. Introduction

With the development of industrialization, metal parts are widely used in all walks of life because of their excellent properties. However, they suffer from severe friction and wear in harsh environments, which leads to energy loss, material loss, and a shorten component life. For example, it has been shown that about 23 % of the total fuel energy loss is directly attributable to frictional contact [1]. About 1/3 of the world's primary energy is consumed during the friction process, and 80 % of machine failures are caused by wear. In countries with a strong manufacturing sector, losses resulting from friction and wear contribute significantly to the country's GDP [2]. Therefore, it is very important to improve the wear resistance of materials. Surface technology can improve the surface tribological properties of parts, prolong their wear life, and reduce economic losses caused by wear [3,4]. The current surface coating methods include: cold spraying [5], electroless plating [6], physical vapor deposition [7], chemical vapor deposition [8], magnetron sputtering [9], peening techniques [10], plasma electrolytic oxidation [11], friction stir welding [4], laser surface alloying [12], and laser cladding(LC) [13]. Table 1 presents the characteristics of various surface coating methods. Among them, LC can prepare coatings that are metallurgically combined with the substrate, which has been widely studied and reported by scholars. At present, there are many LC material systems, the most prominent of which is high-entropy alloys (HEAs). It is a new alloy composed of various primary elements and possesses excellent properties. For example, excellent wear resistance, excellent mechanical properties at high temperatures, excellent ductility and fracture toughness at low temperatures, superparamagnetic and superconductivity [14,15]. Due to these excellent properties, HEAs are emerging as potential replacements for traditional alloy materials in

* Corresponding author. School of Mechanical Engineering and Automation, Northeastern University, Shenyang, 110819, China.
** Corresponding author. State Key Laboratory of Ultra-precision Machining Technology, Research Institute for Advanced Manufacturing, Department of Industrial and Systems Engineering, The Hong Kong Polytechnic University, Hong Kong, 100872, China.
*E-mail addresses:* sy547515291@163.com (S. Yao), zi-bin.chen@polyu.edu.hk (Z. Chen).

https://doi.org/10.1016/j.jmrt.2023.11.138
Received 13 August 2023; Received in revised form 13 October 2023; Accepted 16 November 2023
Available online 26 November 2023

**Table 1**
The surface coating methods and their characteristics.

| Methods | Characteristics |
|---|---|
| Cold spraying | High spraying rate, low residual stress, non-polluting |
| Thermal spraying | A wide range of applications, the controlled coating thickness; the poor bonding strength, porosity and workpiece deformation |
| Electroless plating | Simple process equipment, low processing cost; environmental pollution |
| Vapor deposition | Dense, uniform, the strong bonding force; the expensive equipment, the thin coating thickness |
| Magnetron sputtering | Fast deposition speed, high coating purity, good compactness, good uniformity; low target utilization rate, high equipment cost |
| Plasma electrolytic oxidation | The simple process, non-polluting, large-scale automatic production; the low current efficiency, the high energy consumption |
| Friction stir welding | The convenient operation process, the simple equipment, the low energy consumption, the high efficiency, the low residual stress; the stirring head wear, and the narrow material application range |
| Laser surface alloying | High energy utilization, wide alloy system range; high dilution rate |
| Laser cladding | High energy density, controllable dilution rate, fast processing speed, small heat affected zone, small deformation, and high solidification rate |

harsh environments. HEAs are currently used in aerospace, nuclear fusion reactors, jet turbine blade manufacturing, and other fields [16]. In addition, HEAs also demonstrate broad potential applications in other industrial fields such as electro/thermal catalytic clean energy conversion [17].

For a long time, most conventional alloys have been designed to enhance performance by adding trace elements to main components. In 2004, Yeh et al. [18] proposed a new alloy design concept that has generated significant interest in various fields, namely HEAs, also known as multi-principal component alloys. However, there are many definitions of HEAs today. D.B. Miracle and O.N. Senkov [19] have elaborated on the definition of HEAs in considerable detail, so this article will not repeat it. In most cases, HEAs are claimed to have a high-entropy effect, a sluggish diffusion effect, a lattice distortion effect, and a "cocktail" effect compared with traditional alloys [16]. The high entropy effect, as a representative effect of HEAs, is mainly used to explain the multi-principal solid solution [16]; the sluggish diffusion effect, which is used to describe the formation of nanometer-sized precipitation [16]; the lattice distortion effect to explain the high intensity of HEAs [16]; the "cocktail" effect was first proposed by Indian scholar Ranganatha [20]. This effect emphasizes the unique performance of each element. Excellent materials together will achieve an unexpected synergistic effect, which also significantly improves the flexibility of HEAs' design. However, the first three of the four effects of HEAs are controversial in theory. A large number of research results show that, under the "high entropy effect", HEAs mainly consist of one or more simple solid solutions, namely, face-centered cubic (FCC), body-centered cubic (BCC), or hexagonal close packed (HCP) phases [21–24], sometimes accompanied by a small number of intermetallic compounds. Tong et al. [25] pointed out that slow diffusion facilitates the formation of nanophases. Senkov et al. [26] pointed out that under the influence of the sluggish diffusion effect of HEAs, it may help to form many complex oxides in $NbCrMo_{0.5}Ta_{0.5}TiZr$ alloy and improve the oxidation resistance of the alloys. Yeh et al. [27] found that in the multi-principal Cu-Ni-Al-Co-Cr-Fe-Si alloy system, the XRD strength decreased abnormally due to the different atomic radii of each principal component. Under the severe lattice distortion effect, HEAs exhibit improved hardness [28]. According to the classical tribology theory [29], the wear resistance of materials is related to their hardness. At present, LC-HEACs have excellent wear resistance, which can be attributed to the combined effect of simple solid solution phase of HEAs, hard Laves phase formed in some cases, and severe lattice distortion.

LC, as a surface modification technology, is a multidisciplinary manufacturing process. In this process, the pre-material is added to the substrate and forms a molten pool after laser irradiation. The added material rapidly solidifies, resulting in the formation of a cladding layer. Aside from the ability to prepare a coating for matrix metallurgy, LC has the following advantages: high energy density, controllable dilution rate, fast processing speed, small heat-affected zone, small deformation, good metallurgical combination with the matrix, and fast solidification speed. It can significantly avoid the segregation of elements in the coating and refine the grain structure [30–32]. LC is widely used in preparing functional coatings and repairing damaged parts [33,34].

At present, the processing methods of LC can be divided into two types [35]: One is the LC technology (synchronized LC) which is based on the synchronization of the pre-material and the laser beam. The synchronous LC can be divided into co-axial LC and non-axial LC according to the position of the material flow and the laser beam, as shown in Fig. 1a. At present, the pre-materials used in co-axial LC are mostly powder materials. The pre-materials used in the non-axial LC are filamentous (Fig. 1c) and powdered (Fig. 1d). The working principle of synchronous LC is as follows: using a high-energy laser as the energy source, the metal material fed synchronously is melted and deposited layer by layer according to the predetermined processing path, to realize the preparation of the coating. The other LC method is based on laser additive manufacturing technology (preset LC), in which the laser beam scans according to a pre-planned path to melt the powder materials on the surface of the substrate, as shown in Fig. 1b.

As shown in Fig. 2a, the cross-sectional morphology of the specimen after the laser cladding process is usually divided into four parts [36]: cladding zone, boundary zone, heat-affected zone, and substrate. In the laser cladding process, the dilution rate, which is determined by the LC process parameters, is often used to express the degree of change in the composition of the cladding alloy caused by the compositional mixture with the substrate. As shown in Fig. 2b, $H$ represents the height of the cladding layer, $h$ represents the penetration depth of the substrate, $W$ represents the width of the cladding layer, and the calculation formula of the dilution rate ($\eta$) can be expressed as:

$$\eta = \frac{h}{H+h} \times 100\% \tag{1}$$

If the dilution rate is low, the metallurgical bonding between the cladding layer and the substrate will be poor. If the dilution rate is high, the substrate will be excessively diluted with the coating, weakening the coating properties and increasing the cracking tendency.

The main purpose of this paper is to introduce the applications and research status on wear resistance of laser cladding high-entropy alloy coatings (LC-HEACs). The first section introduces HEAs and LC; the second section introduces the factors affecting the wear resistance of LC-HEACs; the third section introduces LC-HEACs wear-resistant mechanisms; the fourth section introduces the application potential of HEAs coatings in conventional and complex environments with the background of engineering practice; and the last section is conclusion and perspective. In particular, this paper in the second section divides the entire LC-HEACs process into three stages: preparation, cladding, and post-cladding reprocessing stages, as shown in Fig. 3. According to these three stages, the effects on the wear resistance of LC-HEACs are reviewed respectively. The preparation stage includes the HEAs material system, LC process parameter, enhancement particles, and amorphous alloy phase enhancement. The cladding stage includes auxiliary field-assisted cladding. The post-processing stage includes the post-processing of coated samples after cladding.

## 2. Wear resistance of LC-HEACs

Wear is an important failure mode that limits the service life of components in applications such as the automotive industry, the oil and gas industry, and marine equipment. Therefore, it is extremely

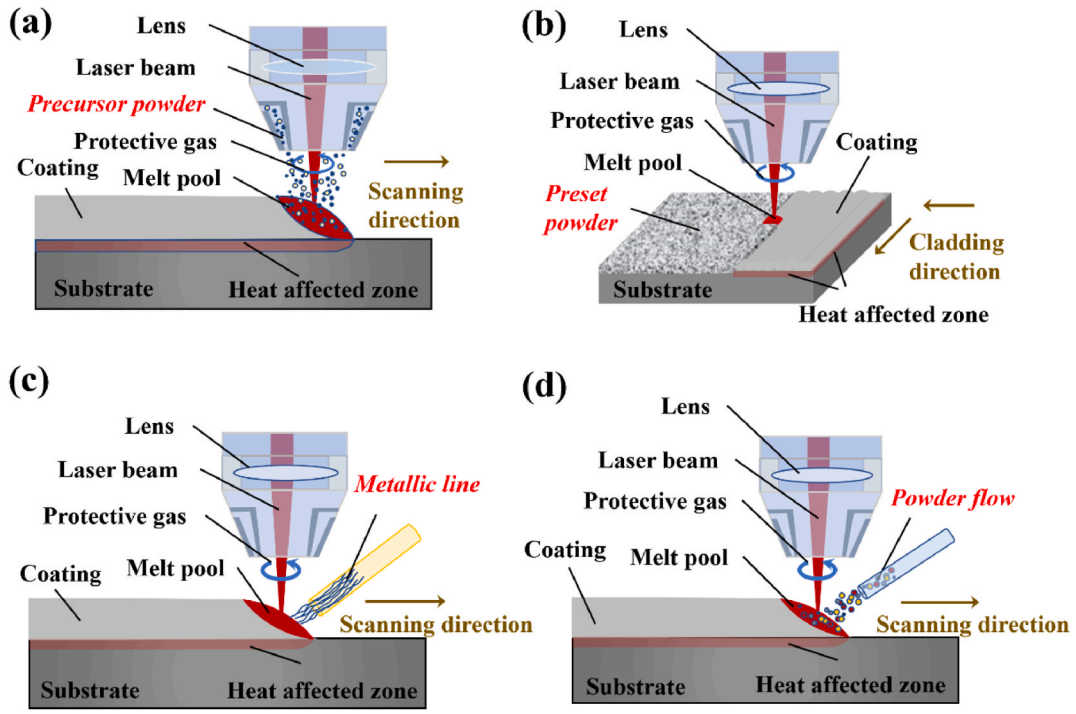


**Fig. 1.** Schematic diagram of the working principle of LC, (a): co-axial LC; (b): preset LC; (c): filamentous material; (d): powder material.

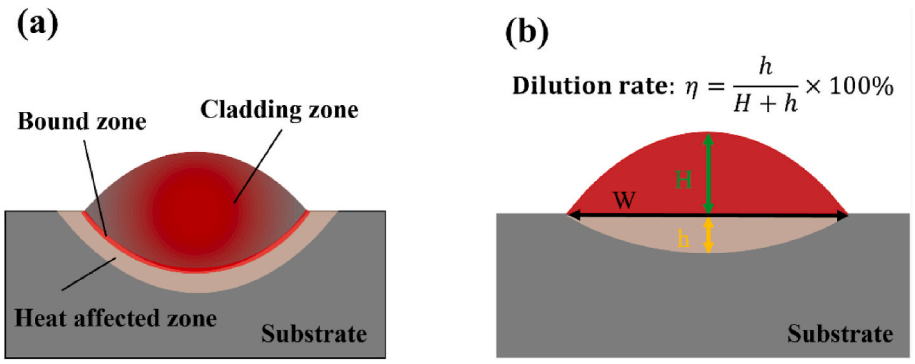


**Fig. 2.** Cross-sectional view of the specimen after cladding, (a): cross-sectional morphology; (b): dilution rate.

important to enhance the wear resistance of the parts. This section will comprehensively introduce the current research status of improving the wear resistance of LC-HEACs from the aspects of HEAs material system, LC process parameters, reinforcement phase, auxiliary cladding, and post-processing.

### 2.1. Effects of HEAs material system

In general, it is well known that the BCC phase has a higher hardness, while the FCC phase has good plasticity. According to Archard's law [29], wear resistance is positively related to hardness. Selecting an appropriate material system and taking advantage of the "four major effects" of HEAs, especially the solid solution strengthening enhanced by the lattice distortion effect on the structure, can improve the hardness of the coating, thereby improving its wear resistance. Therefore, understanding the selection of elements in LC-HEACs, as well as the influence mechanisms of different elements, is instructive for further research on HEAs' wear-resistant coatings. Counting from more than 100 pieces of literature, we summarize the number of times each element is shown in Fig. 4. The existing LC-HEACs material systems primarily encompass two categories: transition metal systems, which consist of transition base metals, and refractory metal systems, predominantly composed of refractory metals, often supplemented by metalloid elements such as B, C, Si, and others.

Among these, the transition metal LC-HEACs material system has received the most extensive attention, featuring elements like Fe, Co, Ni, Cu, Mn, Cr, Ti, and Al. The prominence of this system can be attributed to the exceptional properties exhibited by Fe-Cr-Co-Ni-Mn ("Cantor alloy"), which possesses a single FCC phase structure and showcases remarkable wear resistance. Consequently, there has been a surge in reports exploring variations in the HEAs material system by introducing 1-2 additional elements into the "Cantor alloy", thereby further enhancing the wear resistance characteristics and expanding the scope of LC-HEACs material systems.

The ongoing investigations into LC-HEACs have led to a growing body of literature concerning refractory HEAs. LC-HEACs materials that rely on refractory metals typically consist of a combination of three or more refractory elements, such as Nb, Ta, Mo, W, Zr, Hf, and others. These refractory elements exhibit favorable high-temperature stability, ensuring that refractory HEAs maintain their structural integrity even under elevated temperature conditions. This inherent property renders refractory HEAs highly resistant to wear in scenarios involving high-

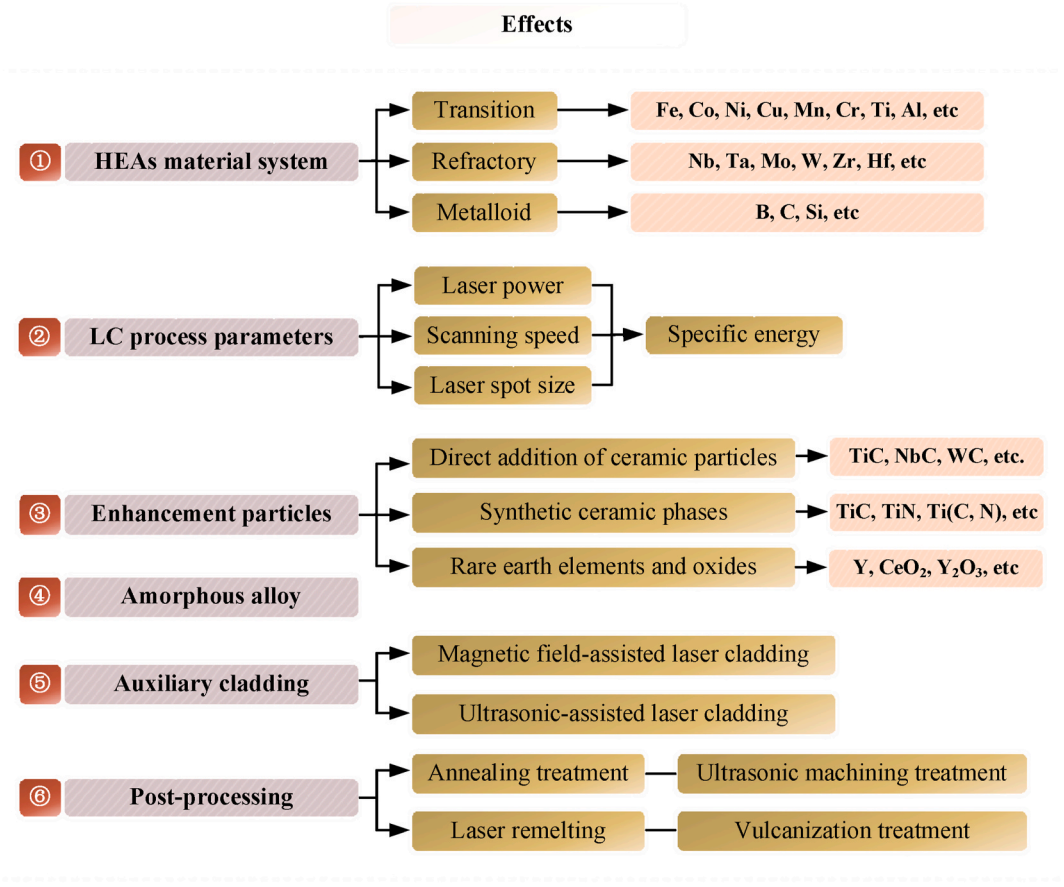


**Fig. 3.** Effects on wear-resistant of LC-HEACs.

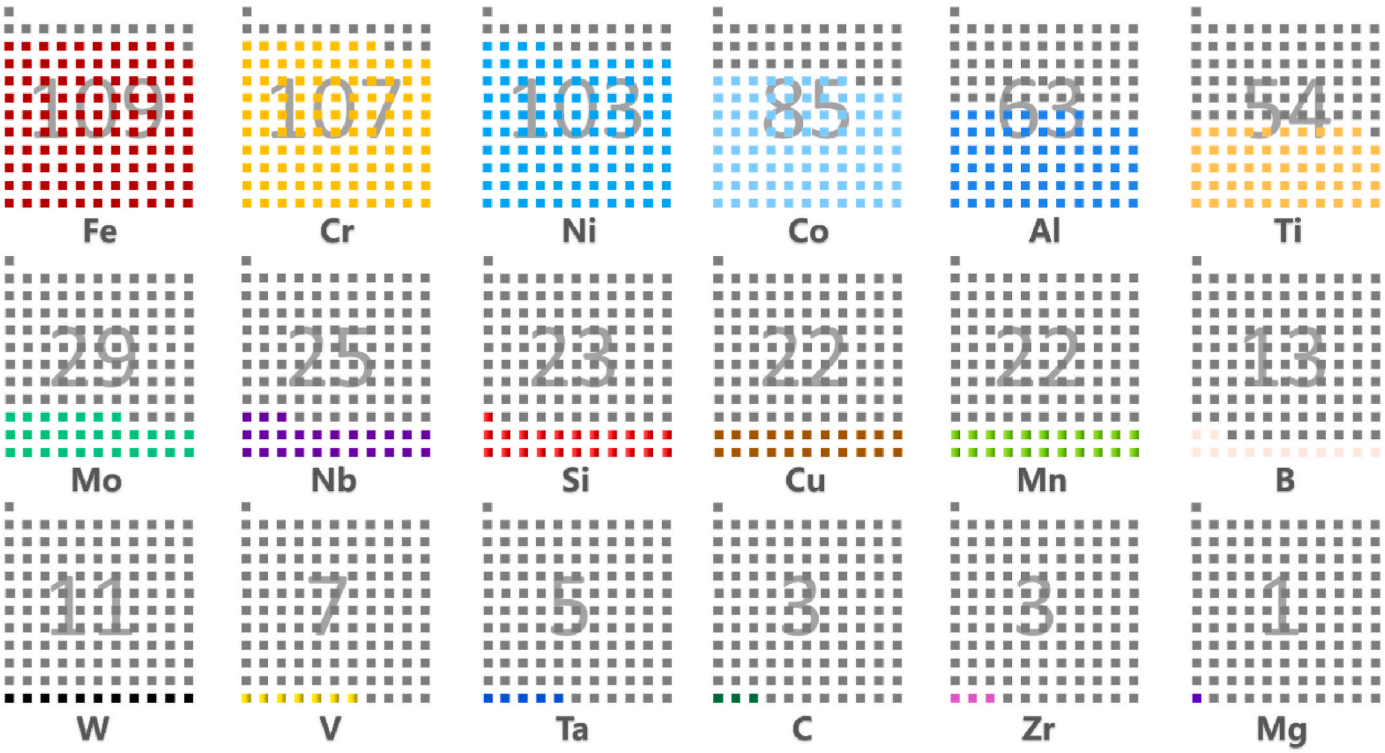


**Fig. 4.** Number of times about different elements used.

temperature friction, thereby establishing promising prospects for their application in high-temperature environments.

Beyond the selection of specific metal types and their combinations, the introduction of non-metallic elements through doping plays a significant role in shaping the properties of LC-HEACs. For instance, the inclusion of elements like C, Si, and B induces alterations in chemical composition and microstructural characteristics, consequently exerting influence over the hardness and wear resistance of the cladding layer. These supplementary elements contribute to the refinement of the base structure of HEAs, enhancing the alloy's overall strength and hardness, thereby optimizing its mechanical attributes and wear resistance.

However, different HEAs material systems will have different influences on the process characteristics of LC. For example, when dealing with refractory HEAs systems, it necessitates a higher laser energy density to ensure complete melting and homogenization. Furthermore, to mitigate oxidation during cladding, a substantial flow of protective gas is essential to establish a conducive protective environment. Conversely, in the case of lightweight HEAs materials, meticulous control of powder feed gas flow is crucial to prevent material dispersion and inadvertent introduction into the molten pool, which could disrupt the formation of the cladding layer. Hence, it becomes imperative to tailor the process parameters and operational techniques according to the specific HEAs material system, thereby guaranteeing process stability and reliability.

Table 2 illustrates the varying wear resistance of different material systems for coatings. In general, the enhancement of performance and process characteristics can be achieved through a judicious combination of metallic elements and the introduction of non-metallic elements. Concurrently, tailored preparation and processing technology schemes need to be meticulously formulated in response to distinct application scenarios and specific challenges that must be addressed. This comprehensive approach serves to advance and facilitate the development and utilization of LC-HEACs.

#### 2.1.1. Transition elements

Ti atoms can effectively dissolve into the FCC matrix and enhance the solid solution-strengthening effect. To study the effect of Ti on the coating, Gu et al. [69] added different contents of Ti into the Co-$Cr_{2.5}$-Fe-$Ni_2$ material system. The results show that the coating without Ti addition is composed of a single BCC phase, and with the increase of Ti content, the coating is composed of BCC and FCC phases. The lattice distortion of the solid solution becomes more serious, which reduces the wear mass loss of the coating. As shown in Fig. 5, the plough grooves generated after wear become narrower and shallower, the surface becomes relatively smooth, and the wear mechanism also changes, transitioning from a mixed mode of micro-cutting and micro-ploughing to micro-cutting. Qiu et al. [70] prepared $Al_2$-Cr-Fe-Ni-Co-Cu-$Ti_x$ (x = 0.0, 0.5, 1.0, 1.5, 2.0) LC-HEACs. With the increase of Ti addition, the proportion of BCC phase and Laves phase in the coating increases, and the hardness of the coating also increases, which increases the wear resistance of the coating. However, when the addition amount of Ti is too high, the coating consists of a single BCC phase, which has a relatively low hardness and a consequent decrease in wear resistance. The coatings showed a tendency that the wear resistance of the coatings first increased and then decreased with the increase of Ti addition. The coating has the best wear resistance when the Ti content is 1.5 at. %, while the wear resistance of the coating is the worst when the Ti content is 2.0 at. %.

Fe is preferred in the selection of HEA materials due to its low price and the addition of Fe can improve the compatibility between the coating and the substrate. By controlling the amount of Fe element in Al-Co-Cr-$Fe_x$-Ni (x = 1.5, 2.5) LC-HEACs, Zhang et al. [57] managed to control the ratio of Fe-Cr-rich disordered BCC phase and Al–Ni-rich ordered BCC phase in the coating, resulting in changing the wear resistance. It can be seen that no cracks, pores, or other defects are found in the coatings, and the coatings have an ideal metallurgical bond with the substrate. At the same time, the upper part of the coating is composed of equiaxed crystals. Compared with the Al-Co-Cr-$Fe_{1.5}$-Ni coating, the Al-Co-Cr-$Fe_{2.5}$-Ni coating exhibits higher strength and better wear resistance due to the different strengthening effects of the precipitates, Zhang et al. [71] showed that different Fe contents would affect the ratio of BCC and FCC phases in the coating by varying Fe amount in $Fe_x$-$Ni_2$-$Co_2$-Cr-Ti-Nb (x = 0.0, 0.5, 1.0, 2.0) LC-HEACs. When the Fe content increases, the FCC phase in the coating decreases, and the BCC phase increases, leading to an increase in the wear resistance of the coating. Among them, the $Fe_2$-$Ni_2$-$Co_2$-Cr-Ti-Nb coating exhibits excellent wear resistance.

Al is an element with a large atomic radius, which can cause serious lattice distortion and significantly improve the coating hardness and wear resistance. Gu et al. [72] discovered a phase transformation from a single-phase BCC structure to a two-phase BCC structure (Mo, Nb-rich) with the increase of Al content in $Al_x$-$Mo_{0.5}$-Nb-Fe-Ti-$Mn_2$ (x = 1.0, 1.5, 2.0) LC-HEACs. The additional Al improves the solid solution strengthening effect while gradually decreasing the -COF)- and wear mass loss of the coating. Among them, the $Al_2$–$Mo_{0.5}$-Nb-Fe-Ti-$Mn_2$ coating has the lowest COF and the least wear quality loss, and this coating has the best wear resistance.

Li et al. [73] investigated the effect of Cu content on $Al_{0.8}$-Cr-Fe-Co-Ni-$Cu_x$ (x = 0, 0.25, 0.5, 0.75, 1.0) LC-HEACs. While the wear rate of the $Al_{0.8}$-Cr-Fe-Co-Ni-$Cu_{0.5}$ coating is only 3.4 % of that of the substrate, it demonstrates excellent wear resistance compared to the substrate. The coating and the substrate exhibit different wear mechanisms, of which the substrate shows delamination fracture and severe adhesive wear and the $Al_{0.8}$-Cr-Fe-Co-Ni-$Cu_{0.5}$ coating shows adhesive wear and abrasive wear.

Ni element is known to benefit the corrosion resistance of materials. To study its performance in wear resistance, Qiu et al. [74] investigated the $Al_2$-Cr-Fe-Co-Cu-Ti-$Ni_x$ LC-HEACs with different amounts of Ni contents. The results show that the appropriate addition of Ni can help to improve the hardness of the coating and thus improve its wear resistance. However, when the amount of Ni is too much (more than 1.0 at. %), the brittleness of the coating increases, resulting in a significant decrease in the wear resistance of the coating.

#### 2.1.2. Refractory elements

Nb with a high melting point (2468 °C) has a large atomic radius, which will cause serious lattice distortion in HEAs, resulting in a significant solid solution strengthening effect. Lin et al. [75] explored the effect of Nb addition on the microstructure and wear resistance of Fe-Co-Cr-Ni-Al-$Nb_x$ (x = 0.0, 0.25, 0.5, 0.75, 1.0) LC-HEACs. The experimental results show that the coating is composed of BCC and FCC phases, and the content of the FCC phase increases with the increase of Nb content. The wear resistance of the coating is positively related to the hardness of the coating, that is, the hardness and wear resistance of the coating first increase and then decrease with the increase of Nb addition. Under the same conditions, the hardness of Fe-Co-Cr-Ni-Al-$Nb_{0.5}$ coating is the highest (773HV) and the wear mass loss is the lowest (1.6 mg). The reason is that when the amount of Nb is moderate, the solid solubility of FCC and BCC will be enhanced, and the hardness and wear resistance of the coating will be improved. However, excessive Nb will cause $Fe_2Nb$ intermetallic compounds in the coating, which will weaken the hardness and wear resistance of the coating.

Mo can form a hard Mo-rich phase or dissolve Mo atoms into the FCC matrix, resulting in higher hardness and wear resistance. Fu et al. [76] successfully configured Co-$Cr_2$-Fe-Ni-$Mo_x$ (x = 0, 0.1, 0.2, 0.3, 0.4) HEAs material systems by changing the amount of Mo added in the Co-$Cr_2$-Fe-Ni system. The results show that the coating is composed of a single FCC phase and a σ-CrMo phase precipitated with the addition of Mo (as shown in Fig. 6), which greatly improves the hardness and wear resistance of the coating in the air. The wear weight loss of Co-$Cr_2$-Fe-Ni-$Mo_{0.4}$ coating is 2.11 mg/h, which is much better than that of the substrate.

**Table 2**
Effects of different material systems on the wear resistance of LC-HEACs.

| HEAs | Main Phases | Substrate | Mode | Parameters | Tribological results of substrates | | | Tribological results of LC-HEACs | | | Ref. |
|---|---|---|---|---|---|---|---|---|---|---|---|
| | | | | | COF | Wear losses | Mechanism | COF | Wear losses | Mechanism | |
| TiVCrAlSi | BCC, IM | Ti6Al4V | Dry sliding | 1000 g (l); (5–15) Hz (f); 60min (t); | N/A | N/A | Abrasive Adhesive | N/A | N/A | Oxidative; Slight chipping and flaking | [37] |
| $Al_2CrFeNiMo_x$ x = 0.5; 1; 1.5; 2.0 | BCC1, BCC2 | Stainless steel | Sliding | 20 N (l); 60min (t); | N/A | ~19 mg | Adhesive Abrasive | N/A | ~13(0.5); 9.8(1.0); 12(1.5); 13(2) mg | N/A | [38] |
| $FeCoCrNiAlTi_x$ x = 0; 0.25; 0.5; 0.75; 1.0 | FCC, BCC1(0); FCC, BCC1, BCC2(0.25, 0.5, 0.75, 1.0) | Q235 steel | Dry sliding | 5Hz (f); 20min (t) | N/A | N/A | Abrasive | 0.45–0.55(0); 0.35–0.45(0.25); 0.25–0.35(0.5); 0.25–0.35(0.75); 0.2–0.3(1.0) | ~3.5(0); 2.5(0.25); 2–2.5(0.5); 1.5–2 (0.75); 1.5–2(1.0) mg | Abrasive (0, 0.25) Slight abrasive (0.5, 0.75, 1.0) | [39] |
| $FeCoCrNiAlB_x$ x = 0; 0.25; 0.5; 0.75 | BCC, FCC, boride (0, 0.25, 0.50, 0.75) | Q235 steel | Sliding | 100 N (l); 100r/min (s); 15min (t) | N/A | N/A | N/A | 0.3–0.4(0); 0.25–0.30(0.25); 0.25–0.30(0.5); 0.20–0.25(0.75); | ~4(0); 2.5(0.25); 2–2.5(0.5); 1.5 (0.75) mg | Adhesive (0); Adhesive and abrasive (0.25, 0.5); Abrasive (0.75) | [40] |
| FeCoCrBNiSi | amorphous, β-Co, γ (Fe, Ni), $Co_2B$ | H13 steel | Sliding | 1150 g (l); 1120r/min (s); 60min (t); Temperature (500 °C) | N/A | 1.3 × $10^{-3}$$mm^3$/(N·m) | N/A | 0.17 | ~6 × $10^{-4}$$mm^3$/(N·m) | Abrasive; Adhesive | [41] |
| CoCrFeNiW | FCC, unmelted W, FCC/ inter-metallics eutectic structures | AISI 1045 steel | Dry sliding | 5 N (l); 600r/min (s); 30min (t); Temperature (600 °C) | N/A | N/A | N/A | N/A | 4.2 × $10^{-5}$$mm^3$/(N·m) | Oxidative wear | [42] |
| $CoCrCuFeNiTi_{1.5}$ | FCC, Laves, Ti-rich | 45 steel | Sliding | 5 N (l); 560r/min (s); 30min (t); Temperature (600 °C) | 0.54 | 2.3 × $10^{-4}$$mm^3$/(N·m) | Oxidative wear, contact fatigue and slight abrasive wear | 0.15 | ~$10^{-5}$$mm^3$/(N·m) | Abrasive and oxidative wear | [43] |
| MoNiTaTiV | BCC, TiN ceramic | GCr15 steel | Dry sliding | 350 N (l); 16 mm/s (s); high-pressure (1507 MPa) | 0.685 | 3.73 $mm^3$ | Abrasive; adhesive and oxidative wea | 0.606 | 2.79 $mm^3$ | Abrasive and slight oxidative wear. | [44] |
| $AlNbMoTaCu_{0.4}$ | BCC, FCC, HCP | Ti6Al4V | Sliding | 20 N (l) | 0.6–0.8 | 9.23 $mm^3$ | Plastic flow accompanied by adhesive wear | 0.2–0.4 | 0.41 $mm^3$ | Slight abrasive | [45] |
| $CoCrFeNiNb_x$ x = 0.45, 0.5, 0.7, 1.0 | FCC, Laves | 304SS | Sliding | 15 N (l); 60min (t) | N/A | 4.5 mg | Adhesive; Delaminated; Oxidative wear | N/A | ~4.4(0.45); 4.3 (0.5); 2.8(0.7); 1.4 (1.0) mg | Abrasive and oxidative and delaminated (0.45, 0.5, 0.7); Abrasive and oxidative (1.0) | [46] |
| $Al_xCoCrFeNi$ x = 0, 0.3, 1.0, 1.5, 2.0 | BCC, FCC (0, 0.3, 1.0); BCC (1.5, 2.0) | Q235 steel | Sliding | 10 N (l); 1000 mm/min (s); 24min (t) | 0.607 | 38.3 × $10^{-6}$$mm^3$/(N·m) | N/A | 0.440(0); 0.378 (0.3); 0.304(1.0); 0.301(1.5); 0.150 (2.0) | 7.27(0); 5.20(0.3); 4.89(1.0); 3.24(1.5); 1.01(2.0) × $10^{-6}$$mm^3$/(N·m) | Oxidation and fatigue wear (0, 0.3, 1.0, 1.5); Abrasive wear (2.0) | [47] |
| $Al_{0.5}CoCrCuFeNi$ | FCC | AZ91D | Dry sliding | 98 N (l); 0.4187 m/s (s); 75min (t) | N/A | 30.38 μg/s | Adhesive | N/A | 11.93 μg/s | Abrasive wear | [48] |
| $Fe_5Cr_5SiTiCoNbMoW$ | BCC | Q235 steel | Sliding | 200 N (l); 200r/min (s); 30min (t) | ~0.4 | 1.04 mg/min | Adhesive | ~0.3 | 0.233 mg/min | Oxidative wear; Adhesive | [49] |
| $AlCoCrFeNiNb_x$ x = 0, 0.25, 0.5, 0.75, 1.0 | BCC, B2 (0); BCC, B2, Laves (0.25, 0.5, 0.75, 1.0) | 304SS | Dry sliding | 10 N (l); 30min (t) | N/A | 0.208 $mm^3$ | Abrasive, supplemented by oxidative and adhesive wear | N/A | 0.161(0); 0.147 (0.25); 0.122(0.5); 0.105(0.75); 0.154 (1.0) $mm^3$ | Abrasive (0, 0.25, 0.5); Slight abrasive (0.75); Adhesive (1.0) | [50] |
| $AlCrFeNi_2W_{0.2}$ $Nb_x$ x = 0.5, 1.0, 1.5, 2.0 | BCC (0.5); BCC, Laves (1.0, 1.5, 2.0) | 304SS | Dry sliding | 10 N (l); 67 mm/s (s); 30 min (t) | 0.85 | ~$10^{-4}$$mm^3$/(N·m) | Adhesive | 0.8(0.5); 0.7(1.0); 0.5(1.5); 0.65(2.0) | ~$10^{-4}$$mm^3$/(N·m) (0.5, 1.0); ~$10^{-5}$$mm^3$/(N·m) (1.5, 2.0) | Adhesive (0.5, 1.0); Abrasive and Oxidative wear (1.5, 2.0) | [51] |

(*continued on next page*)

**Table 2** (*continued*)

| HEAs | Main Phases | Substrate | Mode | Parameters | Tribological results of substrates | | | Tribological results of LC-HEACs | | | Ref. |
|---|---|---|---|---|---|---|---|---|---|---|---|
| | | | | | COF | Wear losses | Mechanism | COF | Wear losses | Mechanism | |
| AlCoCrFeNiTi | BCC, B2, Ti-rich | AISI 1045 steel | Dry sliding | 150 N (l); 60r/min (s); 60min (t) | 0.469 | 36.4 mg | Adhesive | 0.285 | 6.68 mg | Adhesive; Abrasive; Oxidative wear | [52] |
| $FeNiCoCrTi_{0.5}Nb_{0.5}$ | BCC, FCC, Laves | 45 steel | Sliding | 15 N (l); 60r/min (s); 30min (t) | N/A | N/A | N/A | N/A | ~8mg/(N·m) | Abrasive; Slight oxidative wear | [53] |
| $FeCoCrNiMnAl_x$ x = 0, 0.25, 0.5, 0.75 | FCC (0, 0.25, 0.5); BCC, FCC (0.75) | H13 steel | Sliding | 30 N (l); 60min (t) | 0.54 | 10.5 mg | Adhesive | 0.47(0); 0.43 (0.25); 0.41(0.5); 0.37(0.75) | 6.0(0); 4.1(0.25); 3.2(0.5); 1.1(0.75) mg | Gradually changed from adhesive wear to abrasive wear for $Al_0$ to $Al_{0.75}$ | [54] |
| $CoCrFeNiTiAl_x$ x = 0, 0.5, 1.0, 1.5, 2.0 | FCC (0); BCC1, BCC2, Laves (0.5, 1.0, 1.5); BCC1 (2.0) | AISI 1045 steel | Sliding | 10 N (l); 100r/min (s); 15min (t) | 0.54 | 19.7 mg | Abrasive | 0.42(0); 0.28(0.5); 0.31(1.0); 0.33 (1.5); 0.35(2.0) | 4.4(0); 2.9(0.5); 3.7 (1.0); 4.0(1.5); 4.2 (2.0) mg | Abrasive (0); Slight abrasive (0.5, 1.0, 1.5); Microfracture wear (2.0) | [55] |
| $CoCrFeNi_2V_{0.5}Ti_{0.75}$ | BCC, (Co,Ni)$Ti_2$; Ti-rich | Ti6Al4V | Sliding | 15 N (l); 67 mm/s (s); 15min (t) | N/A | ~37.5 × $10^{-5}mm^3$/(N·m) | Abrasive; Oxidative wear | N/A | 4.426 × $10^{-5}mm^3$/(N·m) | Adhesive; Oxidative wear | [56] |
| $AlCoCrFe_xNi$ x = 1.5, 2.0 | disordered BCC (Fe–Cr rich), ordered BCC (Al–Ni rich) | 301SS | Sliding | 5 N (l); 50 mm/s (s); 20min (t) | 0.57 | N/A | N/A | 0.38(1.5); 0.32 (2.0) | 1.79(1.5); 1.09(2.0) × $10^{-3}mm^3$/(N·m) | Abrasive; Oxidative wear | [57] |
| AlCoCrFeNiSi | BCC | AISI 304SS | Sliding | 150 N (l); 150r/min (s); 180min (t) | 0.45 | 4.5 × $10^{-3}mm^3$/(N·mm) | Adhesive; Slight abrasive Oxidative | 0.3 | 4.2 × $10^{-3}mm^3$/(N·mm) | Oxidative wear; Slight adhesive wear | [58] |
| $Fe_{25}Co_{25}Ni_{25}(B_{0.8}Si_{0.2})_{25}$ | FCC, (Fe, Co, Ni)$_2$B; (Fe, Co, Ni)$_3$B | Q235 steel | Sliding | 10 N (l); 80 mm/s (s); 30min (t) | N/A | N/A | N/A | N/A | 4.6 × $10^{-3}mm^3$ | Oxidative; Abrasive | [59] |
| $FeCoNiTiAl_x$ x = 0, 0.5, 1.0 | FCC (0); BCC, FCC (0.5,1.0) | Q235 steel | Dry sliding | 50 N (l); 4Hz (f); 30min (t) | 0.452 | 4.7 $mm^3$ | N/A | 0.408(0); 0.349 (0.5); 0.334(1.0) | 3.5(0); 2.8(0.5); 2.5 (1.0) $mm^3$ | Oxidative and slight abrasive | [60] |
| $AlNbTaZr_{0.8}$ | BCC, HCP | Ti6Al4V | Sliding wear | 10 N (l); 3.6 m/min (s); 120min (t) | 0.82 | 2.41 × $10^{-4}mm^3$/(N·m) | Abrasive | 0.72 | 1.16 × $10^{-4}mm^3$/(N·m) | Slight abrasive and Oxidative wear | [61] |
| $CoCrFeMnTi_{0.2}$ | FCC, Laves | 15CrMn steel | Dry sliding | 80 N (l); 80r/min (s); 120min(t) | N/A | N/A | N/A | 0.37 | 3.596 × $10^{-5}mm^3$/(N·m) | Abrasive and slight oxidative | [62] |
| $Ni_{1.5}CrCoFe_{0.5}Mo_{0.1}Nb_x$ x = 0.55, 0.8 | FCC, Laves | 316SS | Sliding | 10 N (l); 5Hz (f) | N/A | N/A | N/A | ~0.66(0.55); ~0.53(0.8) | ~2.6(0.55); ~2.2 (0.8) mg | Adhesive (0.55) Abrasive and adhesive (0.8) | [63] |
| $FeCoCrNiMoSi_x$ x = 0.5, 1.0, 1.5 | FCC, FeMoSi phases, Si- rich intermetallics | Q235 steel | Sliding | 19.6 N (l); 0.5 m/s (s) | 0.588 | 11 × $10^{-4}mm^3$/(N·m) | Abrasive; Adhesive | 0.360(0.5); 0.375 (1.0); 0.333(1.5) | 0.134 (0.5); 0.107 (1.0); 0.753(1.5) × $10^{-4}mm^3$/(N·m) | Abrasive and adhesive (0.5, 1.0) adhesive and delaminated (1.5) | [64] |
| $AlCrFeNiMn_x$ x = 0, 0.5, 1.0 | BCC, FCC | Pure copper | Sliding | 20 N (l); 300 mm/min (s); 10min (t) | N/A | N/A | N/A | 0.57(0); 0.42(0.5); 0.30(1.0) | 1.23(0); 1.02(0.5); 1.47(1.0) mg | Adhesive (0) | [65] |
| $CoCrCu_{0.7}FeNi_{0.3}$ | FCC | Q235 steel | Dry sliding | 300 rpm (s) temperature (400 °C) | N/A | N/A | N/A | 0.44 | 5.38 × $10^{-5}mm^3$/(N·m) | Slight abrasive and adhesive | [66] |
| NiCoCrMnFe | FCC, Mn | H13 steel | Sliding | 2 N (l); 2Hz (f); 120min (t) | 0.74 | 2.57 × $10^{-5}mm^3$/(N·m) | Direct plough | 0.85 | 9.48 × $10^{-6}mm^3$/(N·m) | Abrasive | [67] |
| $FeNiCoCrMo_x$ x = 0, 0.15, 0.20, 0.25 | FCC | 316SS | Dry sliding | 15min (t) | N/A | N/A | N/A | 0.598(0); 0.590 (0.15); 0.555 (0.20); 0.546(0.25) | 0.36(0); 0.32(0.15); 0.26(0.20); 0.22 (0.25) $mm^3$/(N·m) | Abrasive (0, 0.15); Adhesive (0.2, 0.25) | [68] |

*In parentheses is the corresponding element content. l: Load(N,g); s: Speed(m/s, r/min,* mm/min*); f: Frequency (Hz); t:time (min).*

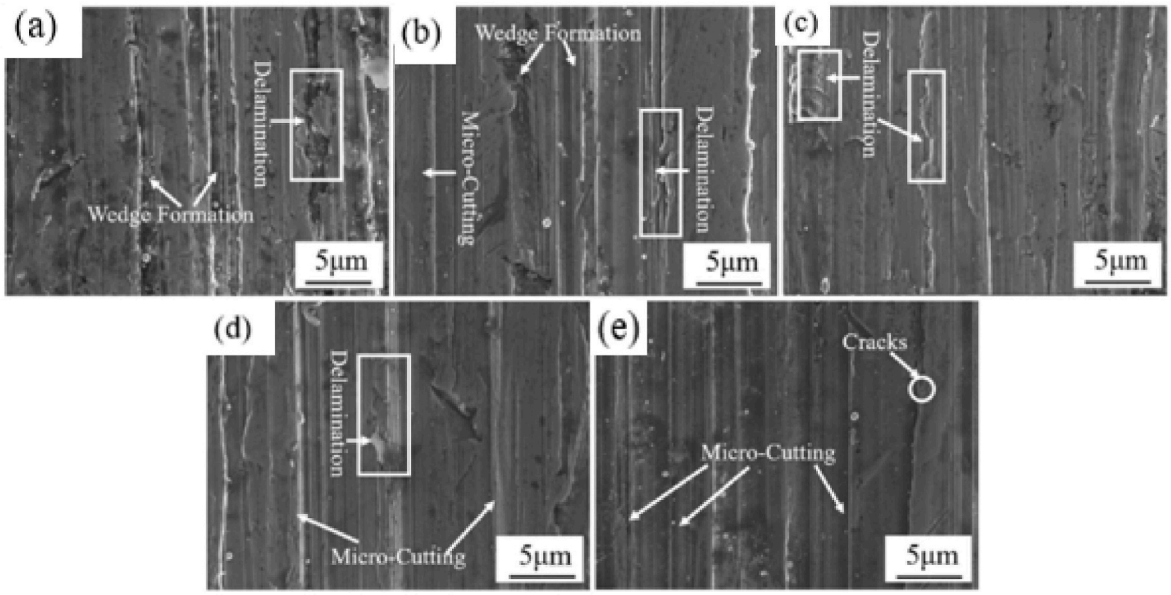


**Fig. 5.** SEM of the wear surface morphology of the substrate and coatings, (a): Q235; (b): $CoCr_{2.5}FeNi_2$; (c): $CoCr_{2.5}FeNi_2Ti_{0.5}$; (d): $CoCr_{2.5}FeNi_2Ti$; (e): $CoCr_{2.5}FeNi_2Ti_{1.5}$ [69].

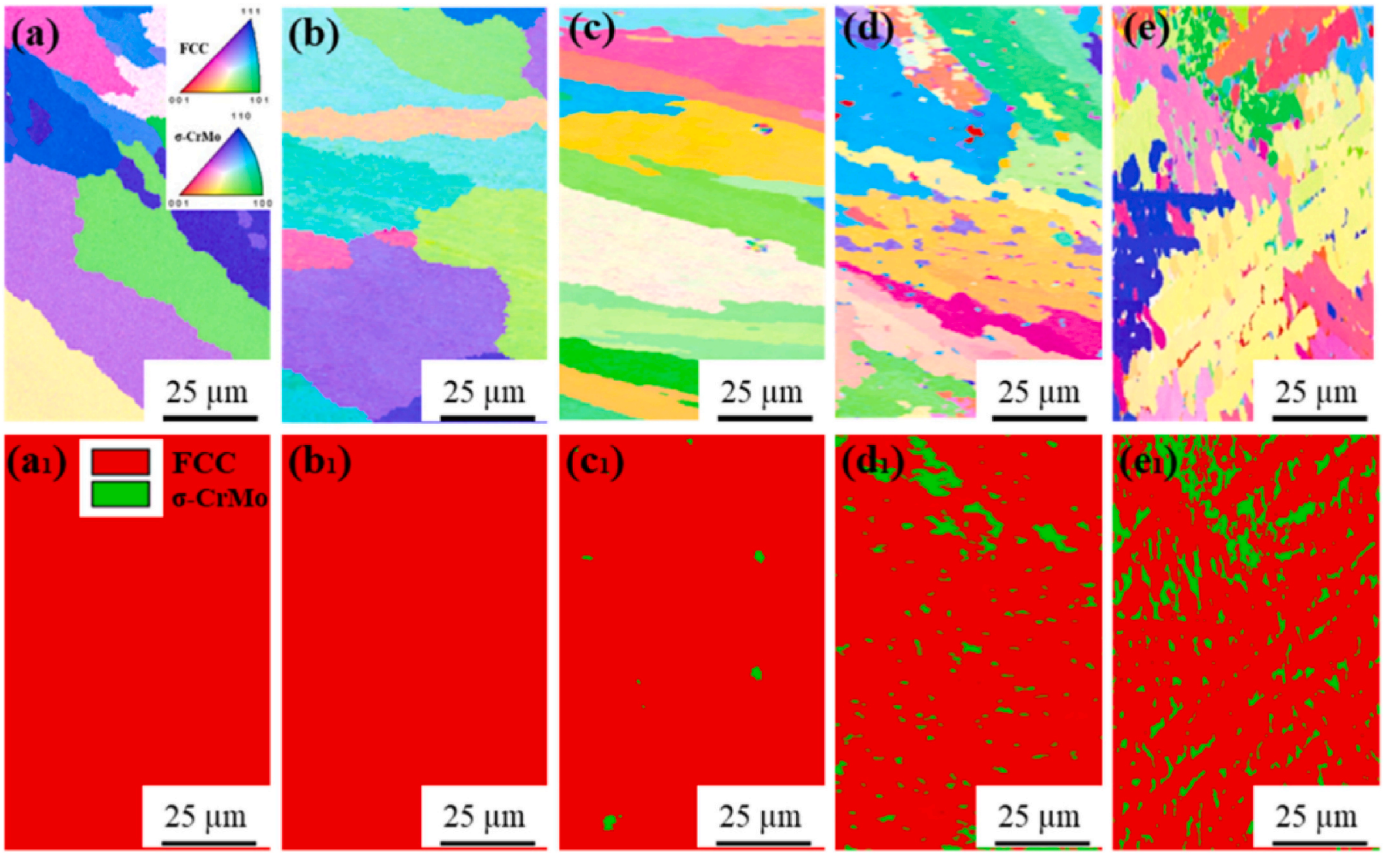


**Fig. 6.** EBSD images of $CoCr_2FeNiMo_x$ (x = 0, 0.1, 0.2, 0.3, 0.4) HEA coatings, (a, a1): $Mo_0$ coating; (b, b1): Mo0.1 coating; (c, c1): $Mo_{0.2}$ coating; (d, d1): $Mo_{0.3}$ coating; (e, e1): $Mo_{0.4}$ coating; (a-e): IPF images; (a1-e1): phase images [76].

To broaden the range of refractory HEAs material systems, Zhao et al. [61] successfully prepared Al-Nb-Ta-$Zr_x$ (x = 0.2, 0.4, 0.6, 0.8, 1.0) LC-HEACs on the surface of Ti6Al4V. The experimental results show that the coating consists of the hexagonal densest structure and the BCC structure. With the increase of Zr content, the hardness of the coating increases correspondingly, thereby improving the micro-cutting resistance of the coating and gradually decreasing the wear rate. However, with the further increase of Zr content, the hardness increases with the sacrifice of ductility and toughness, resulting in the initiation and propagation of cracks in the surface and sub-surface regions of the

coating during fatigue loading. When the addition of Zr increases from 0.2 at. % to 1.0 at. %, the wear resistance of the coating first increases and then decreases, but the wear resistance of all coatings is better than the substrate. The coating has the most excellent wear resistance when the addition amount of Zr is 0.8 at. %. At the same time, the wear mechanism of the coating changes from micro-cutting of Al-Nb-Ta-$Zr_{0.2}$ coating to micro-cutting and oxidation of Al-Nb-Ta-Zr $_{(0.4\sim0.8)}$ coatings, and finally the micro-cutting, oxidation and brittle peeling occur in Al-Nb-Ta-$Zr_{1.0}$ coating.

### 2.1.3. Metalloid elements

Liu et al. [77] investigated the tribological properties of Al-Co-Cr--Fe-Ni-$Si_x$ (x = 0.0, 0.1, 0.2, 0.3, 0.4, 0.5) LC-HEACs with different Si contents. XRD results show that the coatings are composed of a single-phase BCC structure. However, with the addition of Si, the diffraction peak of BCC shifts slightly, because Si atoms replace other atoms in the original BCC solid solution, resulting in the lattice shrinkage. With the increase of Si content, the grains in the coating gradually refine. The grain size reaches the smallest when the Si content is 0.5, as shown in Fig. 7. The coating consists of equiaxed grains and intergranular regions, and nano-particles are found in equiaxed grains, and serious dislocations occur in the equiaxed grains. At the same time, the $Cr_{23}C_6$ precipitation found at the grain boundary helps to refine the growth of the coating grains. Therefore, when the Si content is 0.5, the hardness of the coating reaches the highest under the joint action of dislocation strengthening, solution strengthening, and fine-grain strengthening. With the increase in Si content, the COF and wear rate of the coating decrease significantly, and the wear mechanism of the coating changes. The coating is transformed from the adhesive, abrasive wear, and delamination wear mechanism of Al-Co-Cr-Fe-Ni and Al-Co-Cr-Fe-Ni-$Si_{0.1}$ to oxidative wear and slight abrasive wear when Si addition is 0.2-0.5 at.%. The wear surface of the Al-Co-Cr-Fe-Ni-$Si_{0.5}$ coating is characterized by XPS, and the results show that the surface on which oxidative wear occurs contains $SiO_2$ and SiO that also act as lubricants during the wear process, therefore, the coating has excellent wear resistance.

In addition to Si element among non-metallic elements, B element has also been studied because of its advantages, such as refinement of grain size. Liu et al. [78] prepared Fe-Co-Cr-Ni-$B_x$ (x = 0.5, 1.0, 1.5) LC-HEACs with different B contents on Q245R steel. The test results show that with the increase of B content, the microstructure of the coating is refined, and the wear resistance of the coating is also improved. Aguilar-Hurtado et al. [79] successfully prepared $Fe_{50}$-$Mn_{30}$-$Co_{10}$-$Cr_{10}$ series LC-HEACs with different contents of B element by LC technology, and obtained a similar conclusion.

By changing the material system of the coating, even if the proportion of a certain element is slightly changed, the wear resistance of the coating will be greatly affected, which also highlights the magic of the "cocktail" effect of HEAs. Therefore, the selection and combination of the elements are not arbitrary. It is necessary to select the HEAs material system, the selection of the substrate, and the corresponding cooperation with the LC process parameters according to the actual requirements. Then, the phase structure of LC-HACs was preliminarily predicted by calculating the phase formation rule of multi-partite HEAs.

## 2.2. Effects of LC process parameters

The macroscopic morphology, dilution rate, microstructure, and mechanical properties of the cladding layer are closely related to the LC process parameters. Among them, three important process parameters may affect the quality of cladding: laser power, scanning speed, and laser spot size. In order to obtain a cladding layer with no macroscopic defects, moderate dilution rate, desired microstructure, and excellent mechanical properties, many researchers changed the process parameters and studied the effect of LC parameters on the wear resistance of the coating. Different studies on improving the wear resistance of coatings by changing the parameters are shown in Table 3.

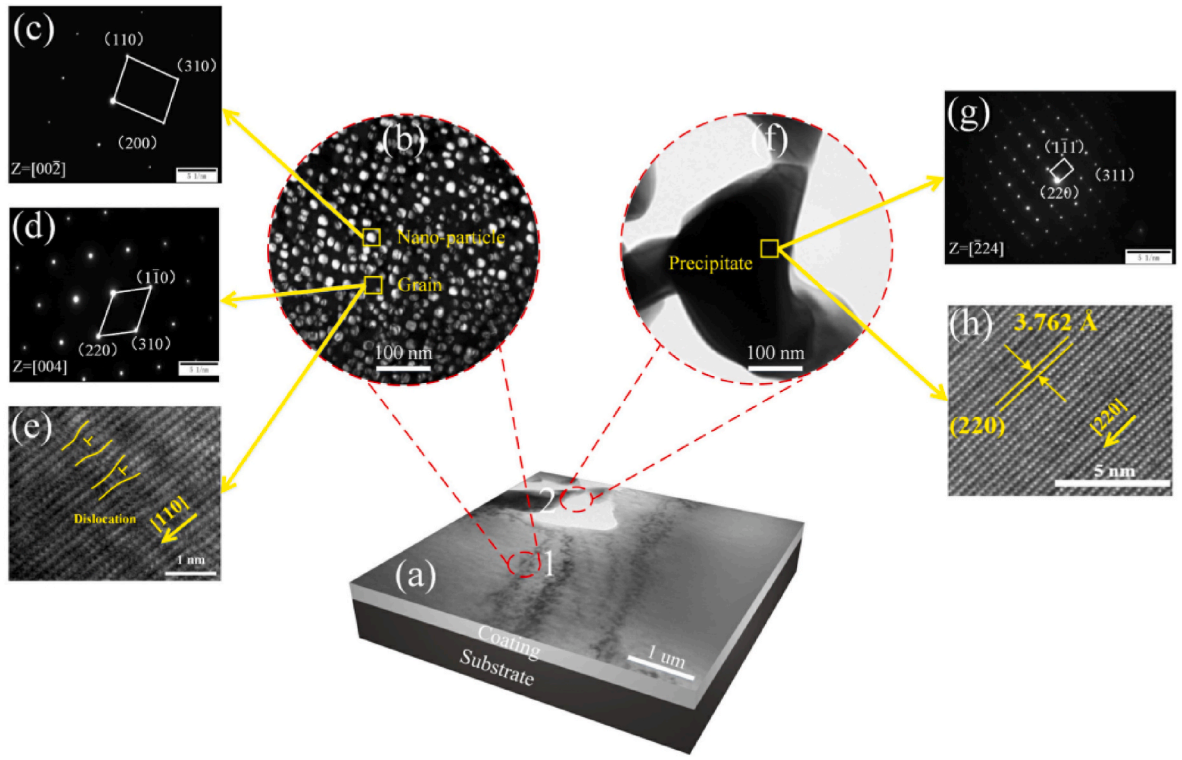


**Fig. 7.** TEM images of the $AlCoCrFeNiSi_{0.5}$ HEA coating, (a): bright field TEM image; (b): magnified image of the Area 1; (c): SAED pattern of the grain; (d): SAED pattern of the particle; (e): HRTEM image of the grain; (f): magnified image of the Area 2; (g): SAED pattern of the precipitate; (h): HRTEM image of the precipitate [77].

**Table 3**
Effects of different process parameters on the wear resistance of coatings.

| Equipment | Laser type | Laser power | Scanning speed | Power density (W/mm$^2$) | Feeding method | Substrate | HEAs | Main phase composition | Tribology results of LC-HEACs | Ref. |
|---|---|---|---|---|---|---|---|---|---|---|
| LMS-50 | $CO_2$ laser | 1.4-1.8 KW | 4 mm/s | 350-450 | Pre-placed powder 1 mm | 304SS | $CoFeNi_2V_{0.5}Nb_{0.75}$ | FCC Laves | The wear resistance increases first and then decreases with the increase of power | [80] |
| LMS-50 | $CO_2$ laser | 1.4-1.8 KW | 4 mm/s | 350-450 | Pre-placed powder 1 mm | 304SS | $CoFeNi_2V_{0.5}Nb_1$ | FCC Laves | The wear resistance increases first and then decreases with the increase of power | [80] |
| YLS-6000 | Fiber laser | 2.4-3.2 KW | 3-5 mm/s | 120-160 | Pre-placed powder 1 mm | M2 tool steel | MoFeCrTiWAlNb | BCC Laves (Nb,Ti)C carbides | When the parameters are 2.6 KW, 4 mm/s, the wear resistance is the best | [81] |
| N/A | Fiber laser | 3-5.5 KW | 30-60 mm/s | 652-1195 | N/A | 42CrMo steel | FeCoCrNiMoC | N/A | When the parameters are 3 KW, 50 mm/s, the wear resistance is the best | [82] |
| N/A | $CO_2$ laser | 1.6-2.2 KW | 13.3 mm/s | N/A | N/A | N/A | AlCrFeNiCu | BCC FCC | The wear resistance is the best when the laser power is 2.0 KW | [83] |
| YLS-5000 | Fiber laser | 3000 KW | 7-21 mm/s | N/A | Pre-placed powder 1 mm | Q235 steel | AlCoCrFeNi | BCC FCC | The wear resistance is the best when the scanning speed is 17 mm/s | [84] |
| SL-80Nd：YAG | Fiber laser | 233, 476, 583, 700W | 10 mm/min | 93-105, 190-216, 233-265, 280-318 | Pre-placed powder 200 μm | H13 steel | CoCrBFeNiSi | Amorphous | The wear resistance is the best when the laser power is 476W | [85] |

#### 2.2.1. Effects of laser power

When the laser power is too small, the local pores and cracks will appear in the cladding layer, resulting in poor metallurgical bonding between the substrate and the coating. However, suppose the laser power is too large. In that case, the dilution rate will increase, and a large number of elements in the matrix will enter the coatings, therefore, decreasing the coatings' properties [36]. Shu et al. [85] reported the existence of amorphous phases in Co-Cr-B-Fe-Ni-Si LC-HEACs on the surface of H13 steel, which was prepared by using different laser powers (233-700W). The laser power affects the dilution rate of the coating and the cooling rate of the molten pool by changing the heat input, thereby affecting the proportion of the amorphous phase (Fig. 8f). The amorphous phase is mainly distributed in the upper part of the coating (Fig. 8a-d), which decreases the microhardness of the coating with the increase of distance from the upper surface (Fig. 8e). At the same time, the friction and wear test results show that coatings with a higher amorphous phase ratio have lower COF and less wear mass loss (Fig. 8g-h).

#### 2.2.2. Effects of scanning speed

Scanning speed plays a similar role as laser power. If the scanning speed is too fast, the alloy powder cannot be completely melted, and a good metallurgical bond cannot be formed between the coating and the substrate. If the scanning speed is too slow, then the powder will be overburned. In addition, the heat input of the substrate will be considerable, which will increase the dilution rate.

In order to study the effect of laser scanning speed on the structure and properties of coatings, Wei et al. [84] designed and fabricated $Al_{16.80}$-$Co_{20.74}$-$Cr_{20.49}$-$Fe_{21.28}$-$Ni_{20.70}$ LC-HEACs by different laser scanning speeds on the surface of Q235 steel. The results show that the coatings are mainly composed of BCC and FCC phases, but the volume fractions of FCC and BCC phases in the coatings with different laser scanning speeds are different. When the laser scanning speed is greater than 11 mm/s, the XRD pattern shows a strong BCC diffraction peak and a weak FCC diffraction peak, and the increase of the laser scanning speed will increase the number of BCC phases. Room-temperature and high-temperature dry sliding friction test results show that a scanning speed of 17 mm/s (V17) leads to low COF and wear rate with excellent wear resistance. The reason is that increasing the laser scanning speed will greatly increase the subcooling of the molten pool, thereby increasing the nucleation rate and refining the grains. Moreover, the proportion of BCC at V17 is high (volume fraction >90 %), and the BCC phase has higher nano-hardness than the FCC phase. Therefore, the increase of the BCC phase can significantly improve the strength and wear resistance of the coating.

#### 2.2.3. Effects of laser spot size

The laser spot size is another important parameter of LC. The laser beam is generally circular, and the width of the cladding layer mainly depends on the spot diameter of the laser beam. As the spot diameter increases, the cladding layer becomes wider. Generally speaking, the quality of the cladding layer is better under the small spot size. As the spot size increases, the quality of the cladding layer decreases, but the diameter of the spot is too small, which is not conducive to obtaining a large-area cladding layer.

To describe their impacts, the concept of specific energy $E_s$ was introduced:

$$E_s = \frac{P}{DV} \tag{2}$$

In the equation (2), $P$ represents the laser power, $D$ represents the diameter of the laser spot, and $V$ represents the scanning speed. To investigate the effect of specific energy on the microstructure and wear resistance of HEA coatings. Wang et al. [96] prepared several Fe-Co-Cr-Ni-Ti (Ti from the substrate) LC-HEACs with different specific energies on a Ti6Al4V substrate. Macroscopically, under different specific energies, the coating exhibits different macroscopic morphologies, among which the specific energy has the greatest influence on the depth of the molten pool. Microscopically, with the increase of specific energy, the coating undergoes a transition from the FCC phase to the BCC phase and Laves phase, which benefits the hardness and wear resistance of the coating. However, with the increase of specific energy, the diffusion of Ti from the matrix to the coating is promoted, which has a certain negative impact on the hardness and wear resistance of the coating. At present, there is no universally applicable theory for the influence of process parameters on LC-HEACs, but the optimal choice is made considering the coating material system, the matrix material, and the actual situation. Therefore, in future research, the theoretical selection of process parameters can be carried out through simulation analysis, thereby reducing the number of pre-experiments and the cost of

**Table 4**
The effects of directly adding reinforcing phase particles on the tribological properties of coatings.

| Substrate | Coating material | Counter part | Tribological experimental parameters | | | Tribology results of LC-HEACs | | | Ref. |
|---|---|---|---|---|---|---|---|---|---|
| | | | Load | Speed | Time (min) | COF | Wear losses | Wear mechanism | |
| 42CrMo | FeCoCrNi+ 20 wt%WC | SiC | 50 N | 9 m/min | N/A | 0.29 | 0.7 × $10^{-5}$mm$^3$ /(N·mm) | Abrasive | [86] |
| 316L | FeCoNiCr+ 60 wt%WC | $Si_3N_4$ | 1000 g | 400 r/min | 30 | 0.474 | 0.041 mm$^3$ | N/A | [87] |
| Q235 steel | AlCoCrFeNi | $Si_3N_4$ | 40 N | 300 mm/ min | 40 | 1.265 | 1.66 mg | Adhesive | [88] |
| Q235 steel | AlCoCrFeNi+10 wt%NbC | $Si_3N_4$ | 40 N | 300 mm/ min | 40 | 1.258 | 1.31 mg | Abrasive | [88] |
| Q235 steel | AlCoCrFeNi+20 wt%NbC | $Si_3N_4$ | 40 N | 300 mm/ min | 40 | 1.023 | 1.05 mg | Abrasive | [88] |
| Q235 steel | AlCoCrFeNi+30 wt%NbC | $Si_3N_4$ | 40 N | 300 mm/ min | 40 | 1.034 | 1.17 mg | Abrasive | [88] |
| AISI1045 steel | $Al_{0.5}$CoCrFeNi $Ti_{0.5}$+2 at%SiC | $Al_2O_3$ | 9.8 N | 200 mm/ min | 20 | 0.36 | 4.3 mg | Adhesive; delaminated and abrasive | [89] |
| AISI1045 steel | $Al_{0.8}$CoCrFeNi $Ti_{0.2}$+2 at%SiC | $Al_2O_3$ | 9.8 N | 200 mm/ min | 20 | 0.31 | 3.1 mg | Adhesive and abrasive | [89] |
| Q235 steel | FeCoCrNiMn$Ti_{0.6}$($B_4C$)$_{0.4}$ | GCr15 | 100 N | 200 r/min | 60 | N/A | 8.5 mg | N/A | [90] |
| Cu–Zr–Cr alloy | FeMnCoCr | Q235 | 15 N | 392.5 mm/s | 25 | 0.35 | 1.68 mg | Abrasive | [91] |
| Cu–Zr–Cr alloy | FeMnCoCr+5 wt%TiC | Q235 | 15 N | 392.5 mm/s | 25 | 0.27 | 1.37 mg | Adhesive | [91] |
| Cu–Zr–Cr alloy | FeMnCoCr+10 wt%TiC+10 wt% CaF2 | Q235 | 15 N | 392.5 mm/s | 25 | 0.16 | 0.89 mg | Adhesive | [91] |
| Cr12MoV die steel | FeCoCrNiAl+5 wt%TiC | Abrasive paper (400#) | 700 g | 65 r/min | 15 | N/A | 1.82 mg | N/A | [92] |
| Cr12MoV die steel | FeCoCrNiAl+10 wt%TiC | Abrasive paper (400#) | 700 g | 65 r/min | 15 | N/A | 1.63 mg | N/A | [92] |
| Cr12MoV die steel | FeCoCrNiAl+15 wt%TiC | Abrasive paper (400#) | 700 g | 65 r/min | 15 | N/A | 1.55 mg | N/A | [92] |
| Cr12MoV die steel | FeCoCrNiAl+20 wt%TiC | Abrasive paper (400#) | 700 g | 65 r/min | 15 | N/A | 1.71 mg | N/A | [92] |
| 45 steel | FeCoCrNiCu + Cf | 316L | 50 N | 50 mm/ min | 30 | 0.546 | 3.7 mg | N/A | [93] |
| Ti-alloy | AlMoTiZrNb | $Si_3N_4$ | 40 N | N/A | 15 | 0.85 | 0.422 mm$^3$ | Oxidative Adhesive | [94] |
| Ti-alloy | AlMoTiZrNb+0.4 at%C | $Si_3N_4$ | 40 N | N/A | 15 | 0.68 | N/A | Adhesive Abrasive | [94] |
| Ti-alloy | AlMoTiZrNb+0.8 at%C | $Si_3N_4$ | 40 N | N/A | 15 | 0.56 | 0.355 mm$^3$ | Adhesive Abrasive | [94] |
| 304SS | CoCrNiMo+1 at%$B_4C$ | $Al_2O_3$ | 30 N | 1HZ | 30 | 0.39 | N/A | Adhesive | [95] |
| 304SS | CoCrNiMo+2 at%$B_4C$ | $Al_2O_3$ | 30 N | 1HZ | 30 | 0.53 | N/A | Abrasive | [95] |
| 304SS | CoCrNiMo+3 at%$B_4C$ | $Al_2O_3$ | 30 N | 1HZ | 30 | 0.56 | N/A | Abrasive | [95] |
| 304SS | CoCrNiMo+4.2 at%$B_4C$ | $Al_2O_3$ | 30 N | 1HZ | 30 | 0.46 | N/A | Fatigue | [95] |

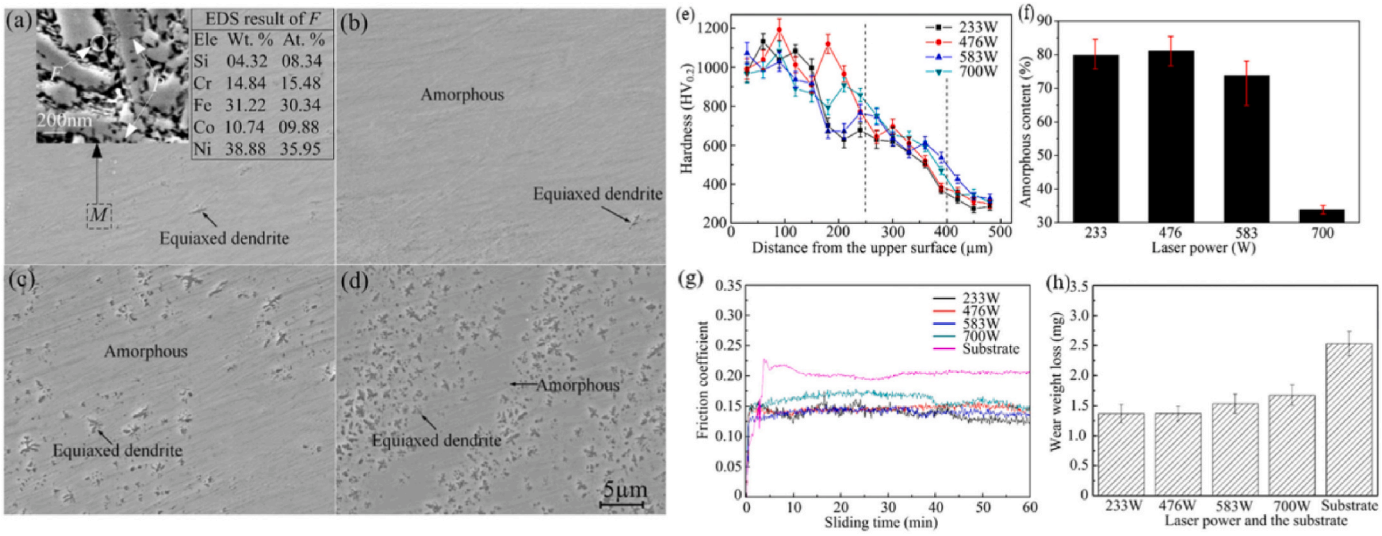


**Fig. 8.** (a-d) Microstructure of the middle and upper layers of the coating at different laser power, (a):233 W; (b): 476 W; (c): 583 W; (d): 700 W; (e): microhardness distribution; (f): the content of amorphous content; (g): COF; (h): wear mass loss [85].

experiments [97].

### 2.3. HEA based coatings

It is found that adding appropriate enhancement elements into the HEAs material system can achieve the second phase strengthening of LC-HEACs and improve the overall properties of LC-HEACs. According to existing literature reports, the reinforcement phases mainly include the direct addition of hard ceramic particles (TiC, NbC, WC, etc.), synthetic ceramic phases (TiC, TiN, Ti(C, N), etc.), and rare earth elements and their oxides.

#### 2.3.1. Direct addition of enhancement phase

Generally speaking, the hardness of ceramics is higher than that of metals. After adding ceramic reinforcing particles, the ceramic particles can effectively inhibit grain growth due to the grain boundary pinning effect and act as a strengthening phase to inhibit the plastic deformation of LC-HEACs. In addition, the protruding ceramic particles during wear reduce the contact area between the coating and the friction pair. Therefore, the mechanical properties, such as hardness and wear resistance of metal materials, can be effectively improved by adding ceramic particles. On the surface of 4Cr5MoSiV1 die steel substrate, Cai et al. [98] successfully prepared Fe-Mn-Cr-Ni-Co + x(TiC) (x = 0 wt%, 5 wt%, 10 wt%, 15 wt%) LC-HEACs, and revealed the tribological behavior of the coating. The results show that adding an appropriate amount of TiC can reduce the COF of the coating and reduce the wear amount, thereby improving the wear resistance of the coating. The wear mechanism changed after adding TiC from adhesive wear (x = 0 wt%, 5 wt%) to abrasive wear (x = 10 wt%, 15 wt%).

In addition to ceramic particles, diamond represents a favored direct reinforcement phase, exhibiting significantly higher strength and hardness than most of metals. Consequently, its incorporation into HEA coatings yields a remarkably hard surface layer, effectively countering friction and wear. The introduction of diamond induces instability in the body-centered cubic solid solution of HEAs, facilitating carbide precipitation and elevating the coating's hardness well above that of the substrate [99,100]. Zhang et al. [101] conducted an experiment involving the fabrication of carbonized HEAs composite coating on 45 steel. They observed that as the diamond content increased, the coating's hardness also increased. Nevertheless, when the diamond content reached 6 wt%, the material's brittleness rose, resulting in cracks and damage during the friction process. Bu et al. [102] prepared diamond-reinforced $FeCoCrNiAl_{0.5}Ti_{0.5}Si_{0.2}$ coating on Ti6Al4V surface. Their investigation revealed that the addition of diamond reduced the dilution rate of the coating, thereby enhancing the metallurgical bonding between the cladding layer and Ti6Al4V. The coating primarily comprised a BCC solid solution, TiC, and $Cr_{23}C_6$ phases. The maximum microhardness of the coating reached 1038.42 $HV_{0.2}$, which was three times greater than that of the substrate. Furthermore, the diamond's excellent thermal conductivity effectively dissipates heat from the coating's surface, preventing heat accumulation and reducing the coating's temperature. Consequently, the introduction of diamond altered the wear mechanism of the coating from adhesive to abrasive wear, ameliorating the wear characteristics of the HEAs coating.

#### 2.3.2. Synthesis of enhanced phase

Adding ceramic particles directly into HEAs sometimes leads to defects such as pores and cracks in the cladding layer. In order to avoid these defects, many scholars improve the tribological properties of LC-HEACs by synthesizing ceramic particles. Guo et al. [103] fabricated in-situ TiN particle-enhanced Co-$Cr_2$-Fe-Ni-$Ti_x$ (x = 0.0, 0.5, 1.0) LC-HEACs on the surface of 904L stainless steel. After adding Ti, the coating consists of irregular dendritic and granular TiN ceramics and a small amount of the Laves phase. With the increase of Ti addition, the wear resistance of the coating is improved. When the Ti addition is 1.0 at. %, the wear of the coating is 1/3 of that of the substrate.

In addition to the TiN phase, the production of TiC through the in-situ synthesis of HEACs also attracts attention due to its excellent contribution to the mechanical properties of the materials. Guo et al. [104] synthesized TiC-enhanced Co-Cr-Cu-Fe-Ni-$Si_{0.2}$ LC-HEACs on the surface of 304 stainless steel. Ti atoms and C atoms are rapidly dissolved in the alloy after being added to the coating materials. TiC particles nucleate rapidly with the rapid reduction of bath temperature. The inter-dendritic zone of TiC is formed and the in-situ reinforced TiC phase is achieved, resulting from the grain boundary diffusion as illustrated in Fig. 9. The tribological test results show that the in-situ synthesized TiC-enhanced coating has excellent wear resistance. It is worth noting that when the amount of Ti and C is too high, the TiC particles in the coating are too large, reducing the number of TiC particles per unit area, which harms the wear resistance of the coating.

TiC and TiN have the same lattice structure and are easily fused to form Ti (C, N). Yan et al. [105] in-situ fabricated Ti (C, N)-enhanced Al-Co-Cr-Fe-Ni-Si LC-HEAC on the surface of H13 steel substrate by LC technique. After a wear test with a normal load of 300 N and a sliding distance of 1400 m, the wear weight loss of the coating is only 12 ± 5 mg, and the small weight loss of the coating indicates its excellent wear resistance. The main wear mechanism of the coating is oxidative wear, accompanied by a small amount of abrasive wear. Table 5 summarizes the effects on the tribological properties of coatings by synthesis of reinforced particles.

Other enhancement phases, such as CNT, Graphene, $TiB_2$, $Al_2O_3$, etc. [111–114] have been reported to have excellent properties. However, few reports are investigating the aforementioned enhancement phase in LC-HEACs. At the same time, $MoS_2$, $WS_2$, and hexagonal boron nitride (hBN) are usually added to the ceramic or metal matrix to produce self-lubricating materials, which significantly improve the tribological properties of the materials [115,116]. However, few studies have been done on incorporating the above materials into LC-HEACs. This is a direction that is worth extensive study.

Intermetallic compounds, such as those with a body-centered cubic and Laves crystal structure, exhibit compact crystal structure and high hardness, rendering them resistant to plastic deformation. Their incorporation into HEAs significantly enhances surface hardness, resulting in improved resistance to abrasion and wear during friction. However, this heightened hardness introduces substantial internal stresses within the HEAs, which may cause material deformation and cracking. Furthermore, intermetallic compounds are inherently brittle, making HEAs prone to cracks and fractures under significant plastic deformation, giving rise to defects like cracks, weak bonding, and deformation. To reconcile this inherent contradiction, a comprehensive approach can be pursued. This strategy encompasses optimizing the phase structure, refining the preparation processes, applying surface treatments and coatings, utilizing buffer materials, adjusting process parameters, and incorporating composite materials. By carefully managing these aspects, materials can attain a balance of appropriate hardness, strength, plasticity, and toughness, thus achieving the dual benefits of superior wear resistance and LC formability.

#### 2.3.3. Rare earth element reinforcement

Rare earth is the collective name of 17 chemical elements of Scandium, Yttrium, and Lanthanide elements in the third subgroup of the periodic table, and generally exists in the form of oxides. Rare earth oxides have excellent physical and chemical properties that are known as the vitamins of metals. Rare earth elements can play an important role in the modification, purification, and alloying of surface-modified materials, and can also limit the growth of nuclei and refine the grains [117]. Therefore, adding an appropriate amount of rare earth elements can improve the quality of the coating and significantly improve the tribological properties of the coating. Gu et al. [118] prepared Mg-Mo-Nb-Fe-$Ti_2$-$Y_x$ (x = 0 %, 0.4 %, 0.8 %, 1.2 %) LC-HEACs on the surface of Q235 steel. The results of friction and wear show that the wear mass loss of the coating decreases with the addition of Y. The surface

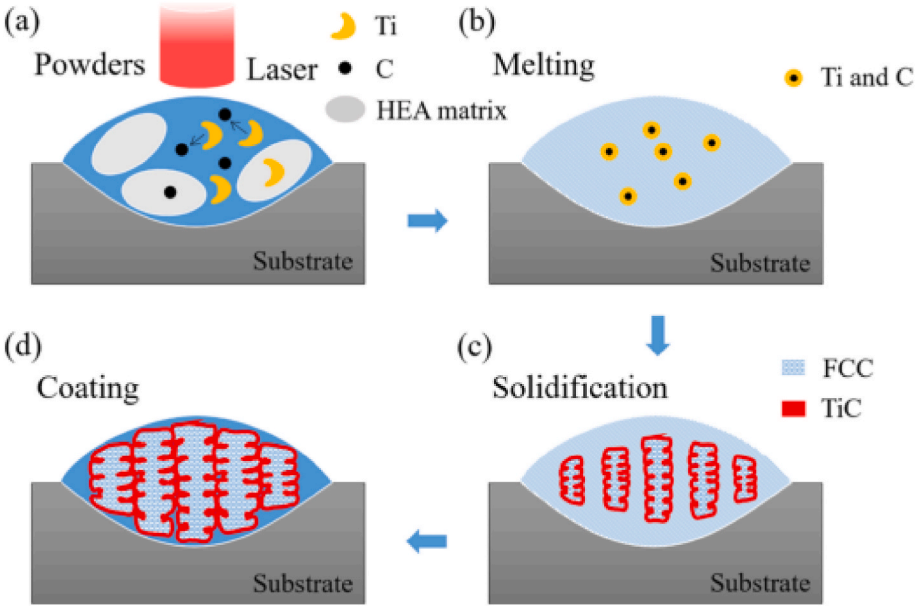


**Fig. 9.** Schematic diagram of in-situ synthesized TiC phase, (a): Original coating material; (b): reaction of Ti and C; (c): growth of TiC phase; (d): TiC and dendrites structure in the coating [104].

**Table 5**
Effects of synthesis of reinforced particles on the tribological properties of coatings.

| Substrate | HEAs | Enhancement particle | Counterpart | Tribological experimental parameters | | | Tribology results of Substrates | | Tribology results of LC-HEACs | | | Ref. |
|---|---|---|---|---|---|---|---|---|---|---|---|---|
| | | | | Load | Speed | Time (min) | COF | Wear losses | COF | Wear losses | Wear mechanism | |
| Ti6Al4V | AlCoCrCuNiTi | TiN | N/A | 200 N | 200 r/min | 60 | 0.62 | N/A | 0.49 | N/A | Adhesive | [106] |
| Ti6Al4V | AlCoCrCuNiTi | TiN | N/A | 300 N | 200 r/min | 60 | 0.65 | N/A | 0.54 | N/A | Adhesive | [106] |
| Ti6Al4V | AlCoCrCuNiTi | TiN | N/A | 200 N | 200 r/min | 60 | 0.62 | N/A | 0.41 | N/A | Adhesive | [107] |
| Ti6Al4V | AlCoCrCuNiTi | TiN | N/A | 300 N | 200 r/min | 60 | 0.65 | N/A | 0.53 | N/A | Adhesive | [107] |
| 904L | $CoCr_2FeNiTi_{0.5}$ | TiN | GCr15 | 200 N | N/A | 15 | 0.663 | 83.55 mg | 0.564 | 43.05 mg | N/A | [103] |
| 904L | $CoCr_2FeNiTi$ | TiN | GCr15 | 200 N | N/A | 15 | 0.663 | 83.55 mg | 0.541 | 30.15 mg | N/A | [103] |
| 40CrNiMo | AlCoCrFeNi - 20 % TiC | TiC | GCr15 | 196 N | 200 r/min | 120 | N/A | N/A | N/A | N/A | Abrasive | [108] |
| 304SS | $CoCrCuFeNiSi_{0.2}(Ti,C)_{0.5}$ | TiC | | 50 N | 100 r/min | 30 | N/A | N/A | 0.507 | 0.75 $mm^3$ | Adhesive Abrasive | [104] |
| 304SS | $CoCrCuFeNiSi_{0.2}(Ti,C)_{1.0}$ | TiC | | 50 N | 100 r/min | 30 | N/A | N/A | 0.604 | 0.42 $mm^3$ | Abrasive | [104] |
| 304SS | $CoCrCuFeNiSi_{0.2}(Ti,C)_{1.5}$ | TiC | | 50 N | 100 r/min | 30 | N/A | N/A | 0.562 | 0.56 $mm^3$ | Abrasive | [104] |
| H13 steel | AlCoCrFeNiSi | Ti(C,N) | GCr15 | 300 N | N/A | 60 | N/A | N/A | N/A | 7~17 mg | Oxidative Abrasive | [105] |
| AISI1045 steel | AlCoCrFeNiTi | TiC | $Si_3N_4$ | 200 g | 500 r/min | 30 | N/A | N/A | N/A | $1.3 \times 10^{-8}$ $mm^3$ $N^{-1}$ $m^{-1}$ | Abrasive | [109] |
| 304SS | $FeCoNiCrMnTi_{1.5}$ | TiN | N/A | 30 N | 3 m/min | 45 | 0.7-0.8 | 0.7-0.8 $mm^3$ | ~0.5 | ~0.1 $mm^3$ | N/A | [110] |

morphology of the coating after wear is shown in Fig. 10. The wear mechanism of the coating is mainly a "cutting mechanism", and the groove width of the coating decreases gradually with the increase of Y content. Therefore, the appropriate addition of rare earth element Y is conducive to improving the wear resistance of the HEAs coating. Liu et al. [119] prepared $Al_{0.5}$-Co-Cr-Cu-Fe-Ni-Si LC-HEACs with and without $Y_2O_3$ addition on H13 substrate. The results show that the cracks and pores in the coating are greatly reduced, the grains are refined, and the hardness and wear resistance are significantly improved after adding $Y_2O_3$.

In addition to the Y element, the Ce element has also attracted a lot of attention because of its good chemical activity, unique electronic structure, and large ionic radius. Shu et al. [120] prepared Co-Fe-Cr-Ni-Si-B LC-HEACs with different amounts of $CeO_2$ on the surface of the H13 steel sheet. The grains in the coating are refined with the addition of $CeO_2$, and they reach a minimum size when the $CeO_2$ is 2 wt %. At this stage, the COF and wear loss of the coating are the lowest, and the wear resistance of the coating is the best. A negative effect will

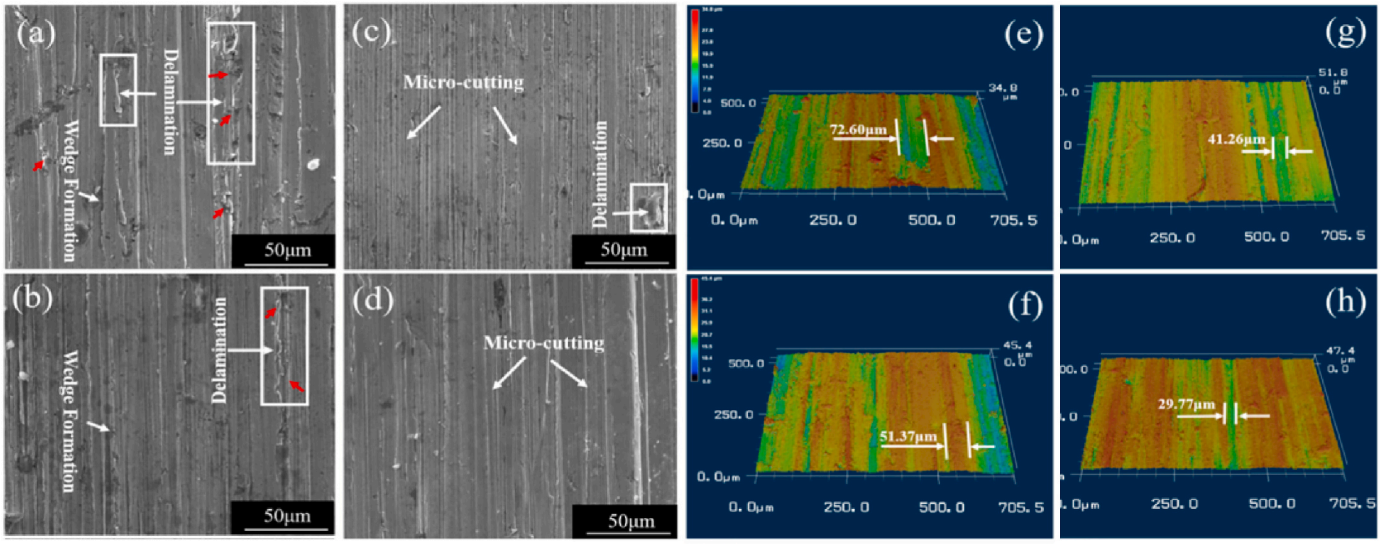


**Fig. 10.** (a–d) 2D wear surface morphology of coatings with different Y content, (a): Y = 0; (b): Y = 0.4 %; (c): Y = 0.8 %; (d): Y = 1.2 %, (e–h) 3D wear surface morphology of coatings with different Y content, (e): Y = 0; (f) Y = 0.4 %; (g) Y = 0.8 %; (h) Y = 1.2 % [118].

dominate when $CeO_2$ (4 wt%) is excessive. A large amount of rare earth compounds will segregate at the grain boundaries, which affects the deformation ability of grain boundaries and aggravates the wear of the coating.

In LC-HEACs, the incorporation of diverse reinforcement materials into the HEAs matrix has demonstrated a substantial enhancement in the coatings' wear resistance. During the LC process, the introduction of rare earth elements into the HEAs coating engenders favorable intermetallic compounds by interacting with the base metal elements. Simultaneously, the addition of rare earth elements contributes to the refinement of the matrix structure, thereby augmenting the material's hardness and wear resistance. Integration of TiC and TiN particles into the HEAs serves to elevate material hardness effectively. Moreover, this inclusion facilitates the formation of a compact protective film on the material's surface, thereby reducing friction and wear incidence. Ceramic particles, characterized by high hardness, exceptional wear resistance, and robust chemical stability, have been integrated into HEAs coatings. This inclusion results in the augmentation of coating hardness and high-temperature performance. In the case of diamond, a natural material renowned for its exceptional hardness, incorporation into the HEAs layer has led to heightened material hardness and the formation of a protective surface film, which in turn reduces friction and wear. Additionally, diamonds can exist within HEAs in the form of single crystals or nanocrystals, affording remarkable wear resistance and high-temperature stability. In summary, the mentioned reinforcement strategies have exhibited promise in enhancing the wear resistance of HEAs. However, it is imperative to recognize that wear resistance represents a composite outcome influenced by factors including material composition, microstructure, hardness, size, distribution of wear-resistant particles, surface roughness, and the prevailing wear environment. Consequently, the extent of wear resistance improvement achievable through various reinforcement methods necessitates further in-depth investigation.

### 2.4. Effects of amorphous

Amorphous alloys have excellent properties such as high hardness and wear resistance, high toughness, and excellent magnetic properties. Some reports have shown that amorphous LC-HEACs can be prepared by combining appropriate elements. Cheng et al. [121] successfully prepared $(Fe_{0.25}\text{-}Co_{0.25}\text{-}Ni_{0.25}(B_{0.7}\text{-}Si_{0.3})_{0.25})_{100\text{-}x}Nb_x$ ($0 \leq x \leq 4$) amorphous LC-HEACs. XRD and TEM results show that the coating can contain an amorphous phase by adding the Nb element appropriately. With the addition of Nb, the FCC grains were refined and the average grain size decreased from 3.5 μm at 0 Nb addition ($Nb_0$) to 1.6 μm at 2.0 at. % Nb addition ($Nb_2$). However, excessive Nb additions will lead to the segregation of bulk Nb in the coating, which will weaken the bonding between the constituent elements, reduce the proportion of the amorphous phase, and finally reduce the overall performance of the coating. The tribological test results show that the $Nb_2$ coating has the lowest wear rate, the narrowest wear width, and the shallowest wear depth.

The preparation of LC-HEACs containing amorphous phases can also be achieved by selecting appropriate LC process parameters. Shu et al. [122] prepared Co-Cr-Ni-Si-B-Fe amorphous coatings using laser power of 520 W, scanning speed of 100 mm/min, and laser beam diameter of 2.2 mm. The resultant coating is composed of (Fe, Co) and (Fe, Ni) solid solutions in the bottom layer and an amorphous phase of up to 85.1 % in the upper layer. The wear mechanisms of the upper and bottom layers are abrasive wear and oxidative wear, respectively. The existence of the amorphous layer significantly reduces the wear amount of the coating and increases the wear resistance.

### 2.5. Effects of auxiliary cladding

By selecting appropriate process parameters, defects such as cracks, pores, and segregation of the coating can be reduced to a certain extent. Many researchers have combined LC with other technologies, such as magnetic field-assisted laser cladding and ultrasonic-assisted laser cladding, to further reduce these internal defects, as shown in Fig. 11.

The magnetic field has the advantages of controlling the crystallization and solidification process of the material, reducing the segregation of components, refining the structure, and improving the properties of the alloy. At the same time, with the assistance of a magnetic field, the uniformity of the microstructure of the coating is improved and the porosity is significantly reduced [123]. Liang et al. [107] fabricated oriented array TiN-enhanced Al-Co-Cr-Fe-Ni-Ti LC-HEACs using a magnetic field-assisted LC technique at a magnetic induction intensity of 1 T. The SEM images of the coating sample are shown in Fig. 12. The coating consists of the dendrite zone, the inter-dendritic zone, and the particle phase zone. Compared with the HEAs coating prepared without magnetic field assistance (0T HEAs coating), the HEAs coating prepared with magnetic field assistance (1T HEAs coating) containing TiN particles that present the "cross" shape of the directional array parallel to the magnetic field direction. The array greatly increases the contact area

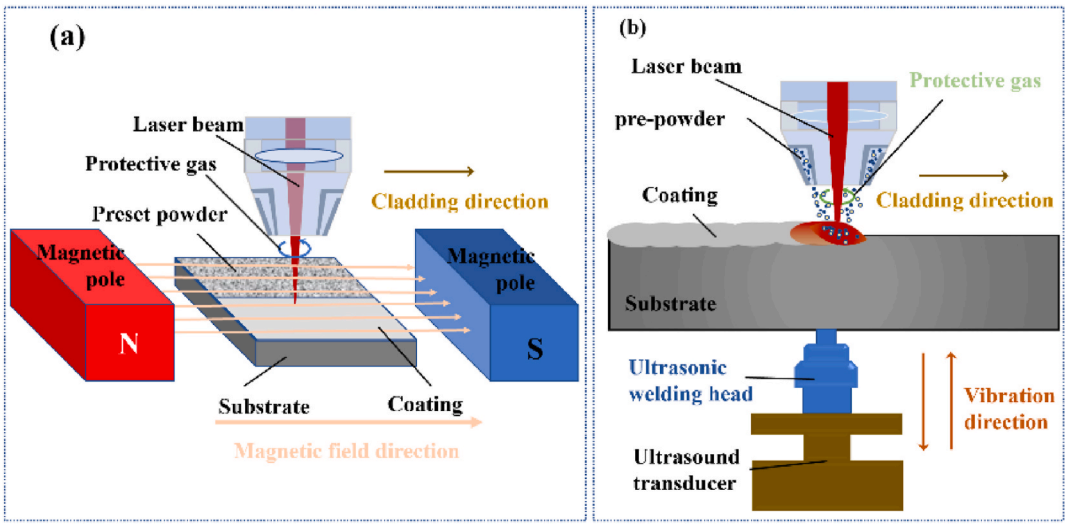


**Fig. 11.** Schematic diagram of the principle of assisted cladding, (a): magnetic field assisted laser cladding; (b): ultrasonic assisted laser cladding.

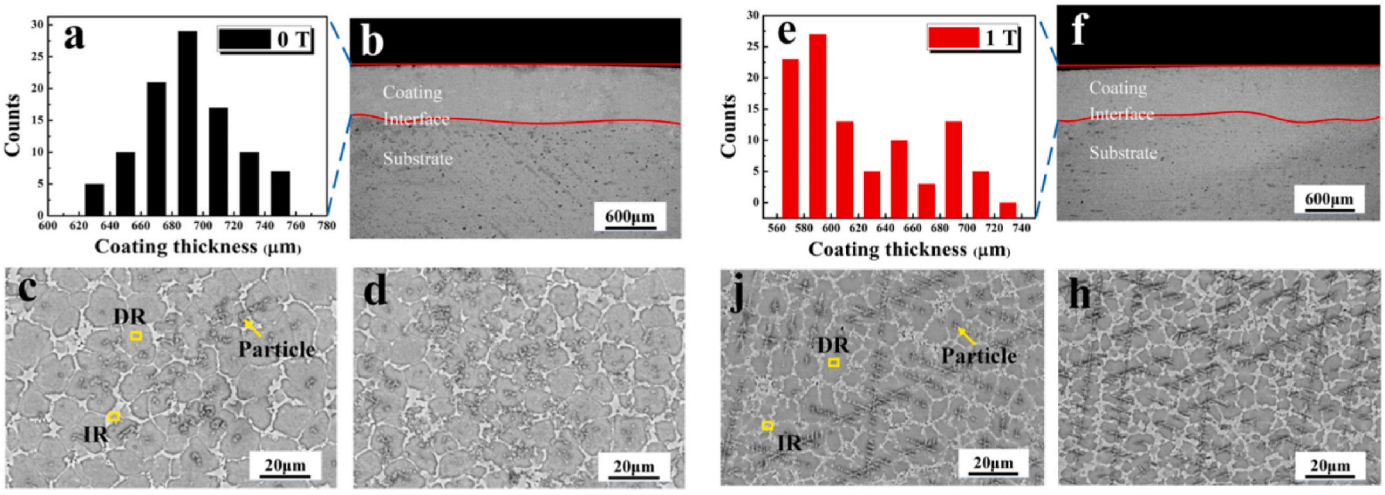


**Fig. 12.** SEM micrographs of HEA coatings with different magnetic induction intensity, (a): thickness; (b): cross section; (c): middle region; (d): top region in the 0 T coating; (e): thickness; (f): cross section, (j): middle region; (h): top region in the 1 T coating [107].

with the dendrite zone and hinders the growth of the dendrite zone, making the dendritic zone size of 1T HEAs coating much smaller than that of 0T HEAs coating. In addition, the grains are refined with the aid of a magnetic field. Tribological experiments indicated that the plastic deformation resistance and ploughing resistance of the coating were improved, owing to the participation of TiN in the wear process. Moreover, the directional array TiN in the coating is large in size, uniformly distributed, and not easy to fall off, possessing high bonding strength that further improves the wear resistance of LC-HEACs. Therefore, the magnetic field-assisted LC-HEACs have better wear resistance than those prepared by conventional methods.

Ultrasonic vibration can promote the full stirring, diffusion, and mixing of various elements in HEAs by causing ultrasonic cavitation, acoustic flow, and mechanical effects, thus, significantly avoiding stress concentration and homogenizing the stress field. At the same time, ultrasonic vibration can also smooth the coating surface and refine the grains in the coating [124]. Wen et al. [125] successfully prepared Fe-Cr-Co-Al-$Mn_{0.5}$-$Mo_{0.1}$ ultrasonic-assisted LC-HEACs, which consist of disordered BCC phase and ordered BCC phase. With the assistance of the ultrasonic field, the growth of grains in the coating is inhibited. The tribological test results show that the COF and wear mass loss of ultrasonic-assisted LC-HEAC are lower than those of the substrate. The wear resistance of ultrasonic-assisted LC-HEACs was 4 times higher than that of the substrate.

### 2.6. *Effects of post-processing after cladding*

The post-processing method was also applied in the cladding samples to reduce the amount of internal structural defects in the coating. The post-processing methods after cladding mainly include: annealing treatment, laser remelting, ultrasonic rolling treatment, ultrasonic impact treatment, and vulcanization treatment.

As a surface post-treatment lubrication technology, ion vulcanization technology can prepare solid self-lubricating film. Cui et al. [126] used ion sulfurizing technology to sulfide LC-HEACs. FeS and FeS + $MoS_2$ polysulfide lubricating films with thicknesses of about 4 μm were prepared on the surfaces of Co-Cr-Fe-Ni-$Si_{0.4}$ and Co-Cr-Fe-Mo-Ni coatings, respectively. The results of tribological experiments show that FeS and $MoS_2$ with dense hexagonal layered structures are generated during the friction process. The layered structure is easily pulverized and adhered to the coating, inhibiting direct contact between the coating and the grinding balls. At the same time, $MoS_2$ is relatively soft and has better viscosity, which extends the life-long usage of the $MoS_2$ film, while the FeS phase is hard and can work in a wide temperature range. During the

wear process, the FeS and $MoS_2$ phases have an effective synergistic effect. The FeS/$MoS_2$ polysulfide film is denser than the FeS mono-sulfide film, which is beneficial to the continuous lubrication of the sulfide layer. Therefore, compared with the single FeS lubricating film, the polysulfide film composed of FeS and $MoS_2$ has a lower coefficient of friction and less wear loss.

Laser remelting is another important post-processing technique to improve the wear resistance of LC-HEACs. Cai et al. [127] combined LC and laser remelting techniques to fabricate Ni-Cr-Co-Ti-V LC-HEACs on the surface of Ti6Al4V. The experimental results show that the coating is composed of (Ni, Co) $Ti_2$ intermetallic compound, the Ti-rich phase, and the BCC solid solution phase. Laser remelting did not change the phase composition of the coating, but the proportion of the Ti-rich phase increased significantly after laser remelting. Compared with LC-HEACs, the coatings after laser remelting have higher microhardness, lower COF, less wear mass loss, and better wear resistance.

The ultrasonic surface rolling process (USRP), as a surface modification technology, refines grains through high strain and high strain rates, thereby enhancing the mechanical properties of coatings. The schematic diagrams of ultrasonic surface rolling are shown in Fig. 13. Cui et al. [128] prepared Cr-Mn-Fe-Co-Ni LC-HEACs by LC technique, and the surface was subjected to USRP at an ultrasonic frequency of 30, 000 Hz. After USRP, a nano-crystalline layer was formed on the surface of the LC-HEACs, and the hardness of the LC-HEACs was greatly improved. Due to the higher hardness, the COF and wear loss of the coating are lower, and the coating exhibits excellent wear resistance.

The effect of heat treatment on LC-HEACs has also been well studied, and some reports have been summarized in Table 6. Guo et al. [129] found that the C14-Laves phase begins to form in the BCC matrix in the Mo-$Fe_{1.5}$-Cr-Ti-W-Al-Nb LC-HEACs when the annealing temperature exceeds 600 °C, which can enhance the mechanical properties of the coating. The wear volume loss of the coating is minimum to about 0.019 $mm^3$ when it was annealed at 650 °C. However, as the annealing temperature increases, the strengthening effect is reduced due to the coarsening of the precipitates.

This section summarizes the latest research progress of LC-HEACs wear-resistant coatings from the aspects of the composition of HEAs, LC process parameters, ceramic particles, amorphous phase, rare earth elements, auxiliary cladding, and post-treatment. Researchers improve the wear resistance of the coating by reducing the cladding defects, refining the cladding grains, and introducing an enhancement phase in the cladding.

## 3. LC-HEACs wear-resistant mechanisms

The friction and wear of materials are affected by various complex factors, including surface finish and working conditions (such as temperature, lubrication, relative surface characteristics, etc.). In addition,

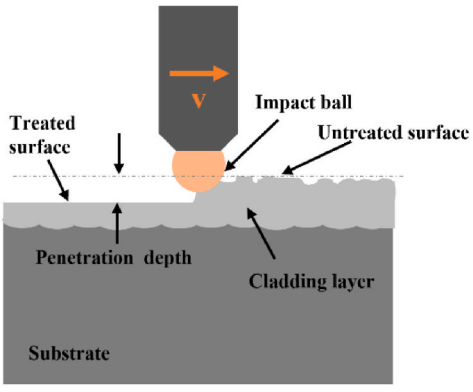


**Fig. 13.** Schematic diagram of the ultrasonic surface rolling post-processing after cladding.

the wear resistance of materials is closely related to the properties of materials, such as hardness, and strength [132]. At the same time, studies have shown that friction-induced uniform plastic deformation of materials during friction and wear can introduce unexpected wear resistance effects [133,134].

The improved substrate wear resistance of LC-HEACs can be attributed to the following two reasons, as shown in Fig. 14. The first reason is that LC-HEACs improve the hardness of the substrate, thereby improving the wear resistance. The second reason is that the surface of LC-HEACs can form a protective friction film.

### 3.1. Hardness effect on wear resistance

Increasing hardness can improve the wear resistance of the coatings. The mechanisms are summarized below.

(1) The HEAs powder in LC-HEACs is rapidly melted and solidified on the substrate under the action of a high-intensity laser beam, which makes the grain growth time in the cladding layer extremely short, and the grain refinement of the entire coating is facilitated by selecting appropriate LC process parameters. At the same time, adding appropriate metal elements to the HEAs material system will further improve the effect of grain refinement strengthening.
(2) Since HEAs contain multiple principal elements, the properties of each element are different, which will lead to a large difference in atomic radius and structure. The solute atoms incorporated into the solid solution cause lattice distortion, which increases the resistance of dislocation movement and makes it difficult to slip, thus increasing the strength and hardness of the alloy solid solution.
(3) The composition of LC-HEACs is often composed of simple FCC or BCC phases, in which the hardness of the BCC phase is higher than that of the FCC phase. Thus, increasing the content of the BCC phase in the coating can increase the hardness of the coating. In some cases, the Laves phase can be generated, and the dispersed hard Laves phase has a second-phase strengthening effect.
(4) Generally, the hardness of ceramic particles is relatively high. Adding appropriate ceramic particles to the HEAs material system can effectively enhance the Orowan strengthening effect of the coating. The uniform dispersion of ceramic-reinforced particles as the second phase particles in the matrix leads to the obstruction of dislocation motion, which is the main reason for the formation of Orowan strengthening.
(5) Amorphous alloys have excellent properties such as high hardness and wear resistance properties. By selecting suitable HEAs process parameters and suitable LC process parameters, a large amount of amorphous phase can be generated in the coating, which can significantly improve the hardness and wear resistance of the coating.

### 3.2. Due to the protective film

In LC-HEACs, an oxide protective friction film containing different elements, such as Al element, Si element, etc., can be formed on the coating surface by selecting the appropriate HEAs main element. This oxide protective friction layer (such as $Al_2O_3$) also acts as a hardness enhancement, thereby increasing the wear resistance of HEAs.

In addition, some post-cladding processing technologies, such as ion sulfurizing technology, can form solid lubricating protective films. The protective films have excellent friction-reducing properties, which can replace lubricating oil and grease under extreme conditions. Thus, the wear resistance of the coating is effectively improved.

**Table 6**
Effects of heat treatment on wear resistance of coatings.

| Substrate | HEAs | Heat treatment | Phase composition | Tribology results of LC-HEACs | | | Ref. |
|---|---|---|---|---|---|---|---|
| | | | | COF | Wear losses | Wear mechanism | |
| AISI1045 steel | $AlCoCrFeNiTi_{0.8}$ | Room temperature | BCC, B2-AlNi, in-situ TiC | 0.64 | $1.36 \times 10^{-6} mm^3/(N{\cdot}m)$ | Abrasive | [130] |
| AISI1045 steel | $AlCoCrFeNiTi_{0.8}$ | Heat treatments (700 °C, 3h) | BCC, B2-AlNi, in-situ TiC | 0.52 | $1.64 \times 10^{-6} mm^3/(N{\cdot}m)$ | Adhesive Oxidative | [130] |
| AISI1045 steel | $AlCoCrFeNiTi_{0.8}$ | Heat treatments (900 °C, 3h) | BCC, B2-AlNi, in-situ TiC | 0.60 | $1.96 \times 10^{-6} mm^3/(N{\cdot}m)$ | Adhesive Oxidative | [130] |
| AISI1045 steel | $AlCoCrFeNiTi_{0.8}$ | Heat treatments (1200 °C, 3h) | BCC, B2-AlNi, in-situ TiC | 0.69 | $6.96 \times 10^{-6} mm^3/(N{\cdot}m)$ | Adhesive Oxidative | [130] |
| M2 high-speed steels | $MoFeCrTiWAlNb_3$ | Room temperature | BCC, MC carbide, C14-Laves | N/A | N/A | Abrasive Adhesive | [131] |
| M2 high-speed steels | $MoFeCrTiWAlNb_3$ | Annealed (950 °C 6h) | BCC, MC carbide, C14-Laves; σ-FeMo | N/A | 0.92 $mm^3$ | Abrasive Adhesive | [131] |
| M2 high-speed steels | $MoFeCrTiWAlNb_3$ | Annealed (950 °C 8h) | BCC, MC carbide, C14-Laves; σ-FeMo | N/A | 0.74 $mm^3$ | Abrasive Adhesive | [131] |
| M2 high-speed steels | $MoFeCrTiWAlNb_3$ | Annealed (950 °C 8h) | BCC, MC carbide, C14-Laves, σ-FeMo | N/A | 0.63 $mm^3$ | Abrasive Adhesive | [131] |

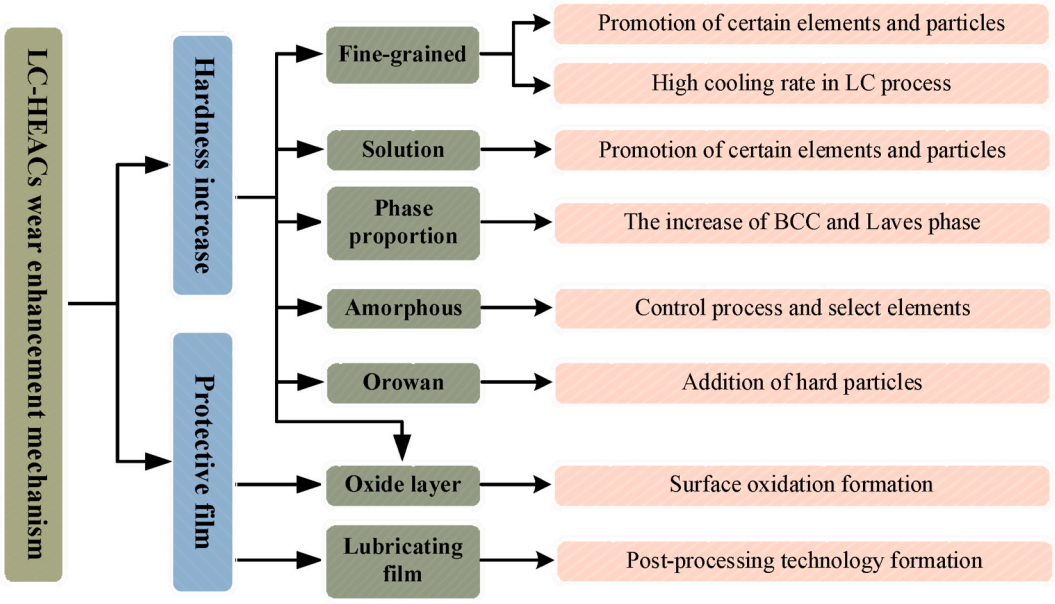


**Fig. 14.** Mechanism of increasing wear resistance of HEAs.

### 3.3. Intrinsic properties of HEAs

The high entropy effect in HEAs enhances the stability of the system and promotes the mixing of constituent elements to form a single solid solution, which shows high strength, high hardness, and excellent wear resistance. Moreover, the variation in atomic radii among elements in HEAs results in lattice distortion, leading to increased hardness, strength, and wear resistance. The lattice distortion effect also influences the bond energy and crystal structure of different elements. During the solidification of HEAs, the phase transition relies on atomic diffusion. In high-temperature regions, the sluggish diffusion effect inhibits phase separation, thereby delaying it until lower-temperature regions are reached. This also prevents grain coarsening and recrystallization to the thermal stability of HEAs. HEAs with a pearlite structure formed through eutectoid transformation maintain this structure's stability at high temperatures due to the slow diffusion effect, thus enhancing the material's overall thermal stability. Therefore, the slow diffusion effect facilitates the formation of supersaturated solid solutions within HEAs. This effect leads to the precipitation of fine nano-phases and sub-crystalline structures on the LC-HEACs. The presence of these nanocrystalline and amorphous states significantly improves the wear and corrosion resistance of the materials.

### 3.4. Characters of LC process

The microstructure of LC-HEACs yields a substantial solution-strengthening effect due to the similarity in the content of principal components. Additionally, LC technology offers several advantageous features, such as ultra-high laser energy density, an ultra-fast cooling rate, and a small heat-affected zone, which complement each other to enhance the coating's toughness. Firstly, the rapid melting and solidification processes during laser cladding refine the material's microstructure, resulting in increased hardness and improved wear resistance. Secondly, LC promotes metallurgical bonding, strengthening the connection between the HEA and the substrate. This enhanced bonding increases overall coating performance, especially when subjected to external loads. Finally, the LC process results in a small heat-affected zone, which effectively reduces thermal stress, residual stress, and deformation. This reduction positively influences the material's wear resistance. However, when utilizing LC technology to prepare HEA

coatings, it is essential to optimize the design based on specific application requirements and working conditions. This optimization includes the selection of appropriate materials, process parameters, and post-treatment techniques to fully leverage the advantages of LC technology for HEA coatings.

### 3.5. Wear condition

LC-HEACs exhibit common wear mechanisms involving abrasive wear, adhesion, and oxidation wear. Variations in wear parameters, including load, speed, frequency, distance, and time, significantly impact the material's surface condition, friction surface temperature, and the behavior of lubricants. As presented in Table 2, under conditions of high speed, heavy load, and high-frequency wear, the wear mechanism of HEAs transitions to more complex wear forms, such as oxidation wear, fatigue wear, and delamination wear. An analysis of Table 4 and Table 5 reveals that the counterpart materials commonly associated with HEAs include GCr15, $Si_3N_4$, $Al_2O_3$, and abrasive paper. These counterpart materials possess different characteristics in terms of hardness, strength, wear resistance, and thermal properties, and they contribute to variations in the wear mechanism. Counterpart materials with high hardness tend to induce abrasive wear during friction, while those with lower hardness are more likely to cause adhesive wear. Additionally, counterpart materials with higher chemical reactivity are prone to atomic diffusion during wear, leading to changes in the surface's chemical composition, as well as alterations in friction coefficient, hardness, and wear resistance. The alteration in wear mechanisms results from a complex interplay of factors related to the wear environment, wear parameters, and material properties. Currently, it remains challenging to systematically elucidate the influence of various factors on wear mechanisms through single-factor experiments. Further in-depth research is needed to provide a comprehensive understanding of these intricate relationships.

## 4. LC-HEACs wear-resistant application

The wear resistance life of parts prepared from common engineering materials is generally not optimized, which has caused great economic losses. Therefore, this section introduces several engineering alloys that are widely used at present and, combined with the practical engineering application background, summarizes the development of HEAs wear-resistant coatings prepared on different engineering alloy material substrates. The wear resistance comparison of several common engineering alloys and LC-HEACs is shown in Table 7.

As a traditional stainless steel material, 316 stainless steel is used in production and life due to its relatively low cost, certain strength, and good machinability. However, its poor surface wear resistance limits its wide application. Therefore, in order to improve the surface wear resistance of 316 stainless steel and expand its application range, Huang et al. [138] prepared Ti-Nb-Zr-Mo LC-HEACs on the surface of 316 stainless steel. The tribological test results show that LC-HEACs have a lower COF and less wear than the 316 stainless steel under the same test conditions, which indicates that the wear resistance of the coating is much better than that of the 316 stainless steel.

45 steel is widely used in machinery manufacturing because of its low cost and good processing performance. However, with the rapid development of the industry, the application environment has put forward higher requirements for surface hardness and wear resistance. It is difficult for ordinary 45 steel to meet the requirements, and it will lead to serious wear and even failure. Therefore, in order to improve the wear life of 45 steel, Qiu [143]. prepared Co-Cr-Fe-Ni-Mo LC-HEACs on the surface of 45 steel by LC technology. The test results show that the wear resistance of LC-HEACs is significantly better than that of the 45 steel.

AISI 1045 steel has good toughness and strength and has been widely used in manufacturing industrial parts such as connecting rods, bolts, gears, and shafts. However, AISI 1045 steel has no poor wear resistance, and it is easy to cause wear and tear during usage. Therefore, it is of great significance to use surface modification technology to improve the surface hardness and wear resistance of AISI 1045 steel. Zhang et al. [139] prepared Fe-Ni-Co-Cr-$Ti_{0.5}$-$Nb_{0.5}$ LC-HEACs on AISI 1045 steel surface by LC technology. The test results show that the coating comprises FCC, BCC, and hard Laves phases. Compared with the substrate, the coating has less wear mass and lower COF.

As hot tool steel, 4Cr5MoSiV (H13) steel has excellent hardenability and hot crack resistance, which is widely used in the manufacture of hot forging dies, hot extrusion dies, and casting dies. However, the severe load of die steel during forging or die casting at high temperatures often causes wear on the die surface, making it unusable for a long time and reducing production efficiency. Shu et al. [144] reported that equimolar Co-Cr-Fe-Ni-B-Si LC-HEACs could significantly improve the service life of the H13 steel. Tribological test results show that the coating has excellent high-temperature wear resistance. Liu et al. [140] pointed out that, under the same conditions, the wear mass loss of the H13 steel matrix (29.8 mg) is three times that of the $Al_2$-Co-Cr-Cu-Fe-Ni LC-HEACs wear mass loss (9.7 mg).

904L stainless steel has excellent strong acid corrosion resistance and is widely used in the stirring blades of phosphoric acid reactors in chemical enterprises. However, during the mechanical stirring process, the 904L stainless steel blades with poor hardness and wear resistance collide violently with phosphate rock, which causes serious corrosion and wear. Lan et al. [145] designed [Al-$(Fe\text{-}Co\text{-}Ni)_{12}$]$Al_x$-$Cr_{3-x}$ (x = 0.0, 0.5, 1.0, 1.5) HEAs material system, and clad it on 904L substrate by LC technology surface to prolong the service life of 904L stainless steel blades and reduce economic losses. Tribological test results show that with the increase of Al content, the wear resistance of the coating increases, and it is far better than that of the substrate. Similarly, Gu et al. [141] prepared $Ni_{1.5}$-Cr-Fe-$Ti_2$-$B_{0.5}$-Mo LC-HEACs on the 904L substrate, which greatly improved the wear resistance of 904L.

Aluminum alloy has become the material of choice for lightweight mechanical design due to its low density, high specific strength, and

**Table 7**
Comparison of wear resistance between common alloys and LC-HEACs.

| Alloys | LC-HEACs | Wear resistance comparison | Ref. |
|---|---|---|---|
| AZ91D | $Cu_{0.5}NiAlCoCrFeSi$ | The wear rate of AZ91D is about 5.3 times that of the $Cu_{0.5}NiAlCoCrFeSi$ coating | [135] |
| 45 | $CoCrCuFeNiTi_{1.5}$ | The wear rate of 45 steel is about 10 times that of the $CoCrCuFeNiTi_{1.5}$ coating | [43] |
| M2 tool steel | $MoFe_{1.5}CrTiWAlNb_3$ | The wear volume of M2 tool steel is about 9.5 times that of the $MoFe_{1.5}CrTiWAlNb_3$ coating | [136] |
| Ti6Al4V | $AlCoCrFeNiTi_{0.5}$ | The wear volume of Ti6Al4V is about 12.7 times that of the $AlCoCrFeNiTi_{0.5}$ coating | [137] |
| 316 SS | TiNbZrMo | The wear mass loss of 316 SS is 3.75 times that of the TiNbZrMo coating | [138] |
| AISI 1045 | $FeNiCoCrTi_{0.5}Nb_{0.5}$ | The wear rate of AISI 1045 is about 2–3 times that of the $FeNiCoCrTi_{0.5}Nb_{0.5}$ coating | [139] |
| H13 | $Al_2CoCrCuFeNi$ | The wear rate of H13 steel is about 3.3 times that of the $Al_2CoCrCuFeNi$ coating | [140] |
| 904L | $Ni_{1.5}CrFeTi_2B_{0.5}Mo$ | The wear mass loss of 904L is about 2.6 times that of the $Ni_{1.5}CrFeTi_2B_{0.5}Mo$ coating | [141] |
| Q235 | $AlCrFeNiW_{0.2}Ti_{0.5}$ | Under the wear experiment with the friction coupled ball of GCr15, the wear rate of Q235 steel is about 30 times that of the $AlCrFeNiW_{0.2}Ti_{0.5}$ coating | [142] |
| SUS 304 | $AlCrFeNiW_{0.2}Ti_{0.5}$ | Under the wear experiment with the friction coupled ball of GCr15, the wear rate of SUS 304 is about 4 times that of the $AlCrFeNiW_{0.2}Ti_{0.5}$ coating | [142] |

sufficient supply. However, due to its low hardness and poor wear resistance, its application is limited in fields with high-reliability requirements. $Al_{0.8}$-Cr-Fe-Co-Ni-$Cu_{0.5}$-based LC-HEACs are prepared with different B [146] and Si [147] contents on the surface of aluminum alloy (5083 aluminum alloy). The test results show that with the increased amount of B and Si, the wear resistance of the coating first increases and then decreases, and when the B content is 0.2 at. %, the coating has the highest wear resistance ($1.5x\ 10^{-7} mm^3/(N{\cdot}m)$). When the Si content is 0.4 at. %, the coating has the highest wear resistance ($2.63x\ 10^{-7} mm^3/(N{\cdot}m)$).

In some cases, parts will be used in harsh environments such as high temperature, strong acid, and strong alkali environments, thus, it is extremely important to improve the tribological properties of the alloy matrix in non-room temperature environments. For AISI 1045 steel, Jin et al. [148] achieved a lower and more stable COF in the Fe-Ni-Co-Al-Cu LC-HEACs compared with the AISI 1045 steel substrate due to the formation of surface oxide films ($Al_2O_3$, $Fe_2O_3$, $Fe_3O_4$, and CuO) at 600 °C and 800 °C, indicating that the coating has the advantage of wear resistance at high temperature. Many critical friction components in offshore engineering equipment, such as valves, pumps, propellers, shafts, and gears, usually work directly in extreme marine environments, which are prone to serious wear and tear, limiting work efficiency and reliability. Liang et al. [142] prepared Al-Cr-Fe-Ni-$W_{0.2}$-$Ti_{0.5}$ LC-HEACs on the surface of Q235 steel. Tribological experiments were carried out with $Si_3N_4$, GCr15, and YG6 balls in seawater conditions. The experimental results show that the friction-coupled balls have a great influence on the friction behavior of the Al-Cr-Fe-Ni-$W_{0.2}$-$Ti_{0.5}$ coating in seawater. When the coupled ball is $Si_3N_4$, the wear mechanism is abrasive wear (as shown in Fig. 15a and b). When the coupled ball is YG6, Mg $(OH)_2$, $CaCO_3$, metal oxides, and hydroxides are formed on the surface of LC-HEACs (as shown in Fig. 15c). These tribo-chemical reactions change the geometry of the worn surface and result in surface polishing, which changes local contact stress and hinders the formation of grooves and cracks, thereby reducing the wear and friction of the specimen, and the resulting coating wear surface is relatively smooth. At the same time, when the LC-HEACs are reciprocating sliding by the YG6 coupled ball, a protective friction film is formed on the wear surface, which will effectively hinder the direct contact between the wear surface of the coating and the YG6 coupled ball, which further reduces the wear rate of the coating (as shown in Fig. 15d). Compared with Q235 steel and SUS304 (typical materials used in seawater environments), LC-HEACs showed better tribological properties when tested with different friction-coupled balls. It shows that LC-HEACs have great application potential in improving the wear resistance of parts in seawater environments. The tribological behavior of LC-HEACs in different environments is shown in Table 8.

## 5. Conclusion

In this paper, the recent research progress of LC-HEACs wear-resistant coatings is reviewed. The research status of LC-HEACs in the field of wear resistance is introduced in detail from five aspects: HEA material system, LC parameters, second-phase enhancement, auxiliary cladding, and post-processing. The main conclusions of this paper are as follows.

(1) By selecting an appropriate material system, one can harness the intrinsic attributes of HEAs, which encompass the high-entropy effect facilitating the formation of a simple solid solution phase, the lattice distortion effect bolstering the mechanical properties of HEAs, and the synergistic "cocktail" effect that reflects the distinctive characteristics of each constituent element within HEAs. According to current literature, there has been extensive documentation on HEAs material systems, building upon the foundation laid by the "Cantor alloy" that modifies one to two elements within the system. Additionally, there is a burgeoning body of research reports focusing on refractory HEAs systems.

(2) The LC process parameters wield a substantial influence over the macroscopic morphology and microstructure of LC-HEACs. The judicious selection of appropriate process parameters can markedly enhance the wear resistance of the coating. Nevertheless, in

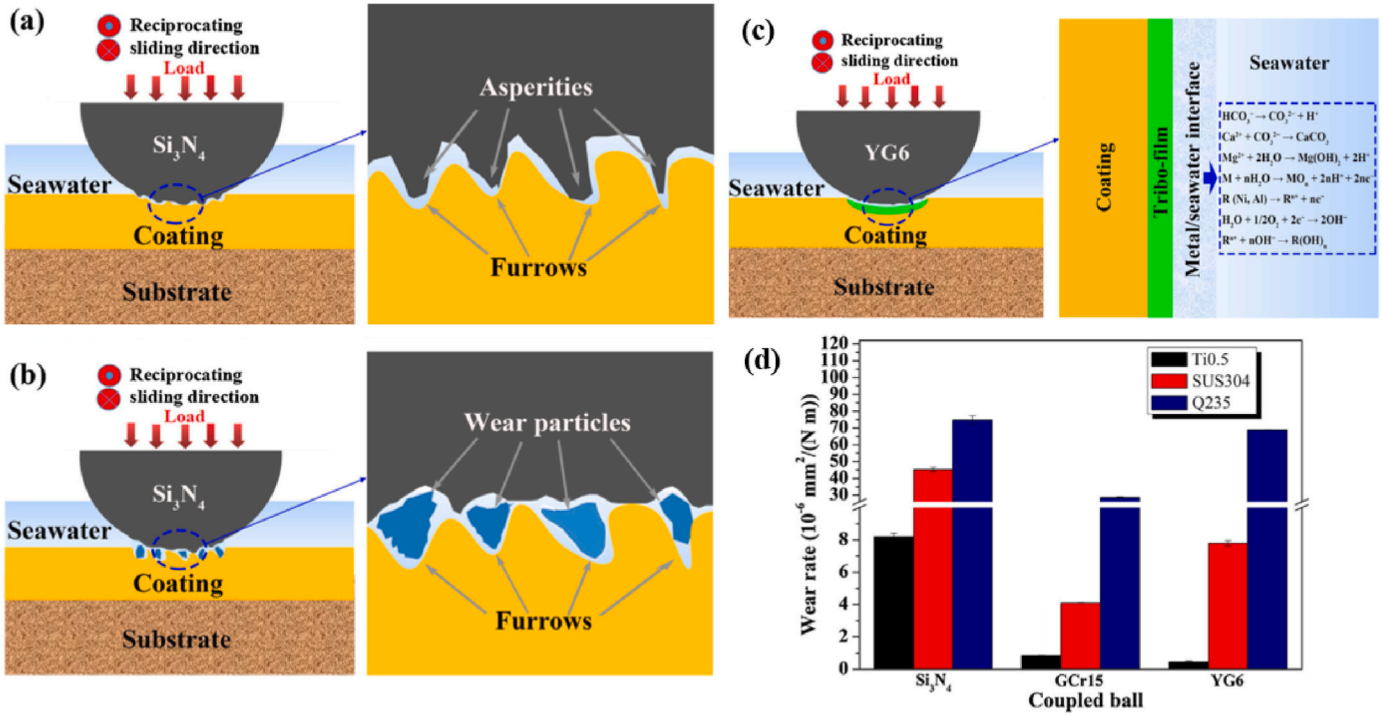


**Fig. 15.** Tribological behavior of HEAs coating, Q235 Steel and SUS304 on different coupled balls in artificial seawater, (a): schematic diagrams of two-body abrasion wear mechanism of HEA coating sliding against $Si_3N_4$ ball; (b) schematic diagrams of three-body abrasion wear mechanism of HEA coating sliding against $Si_3N_4$ ball; (c): schematic diagram of wear mechanism of HEAs coating sliding against YG6 ball; (d): wear rates [142].

**Table 8**
Tribological behaviors of LC-HEACs in different environments.

| Substrate | HEAs | Experimental environment | Counterpart | Tribology results of Substrates | | | Tribology results of LC-HEACs | | | Ref. |
|---|---|---|---|---|---|---|---|---|---|---|
| | | | | COF | Wear losses | Wear mechanism | COF | Wear losses | Wear mechanism | |
| AISI1045 steel | FeNiCoAlCu | 20 °C | WC | N/A | N/A | N/A | 0.8–0.9 | N/A | Abrasive Oxidative | [148] |
| AISI1045 steel | FeNiCoAlCu | 200 °C | WC | N/A | N/A | N/A | 0.8–0.9 | N/A | Abrasive Oxidative | [148] |
| AISI1045 steel | FeNiCoAlCu | 400 °C | WC | N/A | N/A | N/A | 0.8–0.9 | N/A | Abrasive Oxidative | [148] |
| AISI1045 steel | FeNiCoAlCu | 600 °C | WC | N/A | N/A | N/A | ~0.3 | N/A | Abrasive Oxidative | [148] |
| AISI1045 steel | FeNiCoAlCu | 800 °C | WC | N/A | N/A | N/A | ~0.3 | N/A | Abrasive Oxidative | [148] |
| 316 L | AlCoCrFeNi | 25 °C | $Al_2O_3$ | N/A | N/A | N/A | 0.9–1.0 | $12.47 \times 10^{-5}$ $mm^3/(N·m)$ | Oxidative | [149] |
| 316 L | AlCoCrFeNi | 650 °C | $Al_2O_3$ | N/A | N/A | N/A | N/A | $22.95 \times 10^{-5}$ $mm^3/(N·m)$ | Plastic deformation | [149] |
| Ti6Al4V | TiAlNiSiV | Room temperature | $Si_3N_4$ | 0.37 | 10.25 $mm^3$ | Abrasive; Adhesive; Oxidative | 0.45 | 2.54 $mm^3$ | Abrasive Oxidative | [150] |
| Ti6Al4V | TiAlNiSiV | 800 °C | $Si_3N_4$ | 0.35–0.45 | 34.05 $mm^3$ | Abrasive; Fatigue spalling; Oxidative | 0.2–0.3 | 8.34 $mm^3$ | Abrasive Oxidative | [150] |
| Q235 steel | $AlCrFe_2Ni_2W_{0.5}Mo_{0.75}$ | Artificial seawater | YG6 | 0.42–0.44 | N/A | N/A | 0.27 | $10.13 \times 10^{-6}$ $mm^3/(N·m)$ | Abrasive | [151] |
| Q235 steel | $AlCrFe_2Ni_2W_{0.5}Mo_{0.75}$ | 3.5 wt%NaCl | YG6 | 0.32–0.34 | N/A | N/A | 0.32 | $17.82 \times 10^{-6}$ $mm^3/(N·m)$ | Abrasive | [151] |
| Q235 steel | $AlCrFe_2Ni_2W_{0.5}Mo_{0.75}$ | Deionized water | YG6 | 0.34–0.38 | N/A | N/A | 0.38 | $23.89 \times 10^{-6}$ $mm^3/(N·m)$ | Abrasive | [151] |
| Q235 steel | $AlCrFeNiW_{0.2}Ti_{0.5}$ | Artificial seawater | $Si_3N_4$ | ~0.7 | N/A | N/A | 0.52 | $8.19 \times 10^{-6}$ $mm^3/(N·m)$ | Abrasive | [142] |
| Q235 steel | $AlCrFeNiW_{0.2}Ti_{0.5}$ | Artificial seawater | GCr15 | 0.5–0.6 | N/A | N/A | 0.32 | $8.5 \times 10^{-7}$ $mm^3/(N·m)$ | Adhesive | [142] |
| Q235 steel | $AlCrFeNiW_{0.2}Ti_{0.5}$ | Artificial seawater | YG6 | 0.4–0.5 | N/A | N/A | 0.16 | $4.5 \times 10^{-7}$ $mm^3/(N·m)$ | N/A | [142] |
| Ti6Al4V | $CoCrFeNiMo_{0.2}$ | 600 °C | $Si_3N_4$ | 0.17 | $5.83 \times 10^{-4}$ $mm^3/(N·m)$ | Oxidative and brittle debonding | 0.154 | $2.08 \times 10^{-4}$ $mm^3/(N·m)$ | Abrasive | [152] |
| 316 L | AlCrFeMnNi | 400 °C | $Al_2O_3$ | N/A | N/A | N/A | 0.48 | $1.246 \times 10^{-4}$ $mm^3/(N·m)$ | Oxidation Adhesive | [153] |
| 316 L | AlCrFeMnNi | 600 °C | $Al_2O_3$ | N/A | N/A | N/A | 0.63 | $3.172 \times 10^{-4}$ $mm^3/(N·m)$ | Contact fatigue Oxidation | [153] |
| H13 steel | $FeCoCrNiMnAl_{0.75}$ | 600 °C | YG6 | N/A | N/A | N/A | 0.7982 | 4 mg | Oxidative Abrasive | [154] |

the context of diverse HEAs material systems, substrate variations, and specific LC equipment configurations, there is a lack of fixed, universally applicable LC process parameter ranges. Instead, the choice of LC process parameters exhibits a notable degree of flexibility.

(3) The reinforcing phase plays a crucial role in grain refinement within the HEAs coating. It effectively restrains crystal nucleus growth, consequently contributing to the enhancement of wear resistance. In cases where a high-hardness ceramic reinforcing phase is employed, the wear resistance of LC-HEACs can be further elevated.

(4) The utilization of auxiliary cladding and post-processing technologies offers a means to mitigate coating defects resulting from LC methods. These technologies effectively reduce component segregation in HEAs coatings, refine grain structures, and ultimately enhance the wear resistance of LC-HEACs.

## 6. Perspectives

Based on the recent research findings of LC-HEACs, this section identifies prevailing issues within the context of LC-HEACs' application environments, the synergistic influence of LC-HEACs on wear and corrosion, HEA material systems, and LC process parameters. Furthermore, it elaborates on potential future development trends.

(1) Currently, the majority of research concerning the wear-resistant characteristics of HEAs is predominantly limited to experimental conditions conducted at room temperature. As industrial demands grow, an increasing number of components are required to operate in intricate and challenging environments, including those characterized by elevated temperatures, high acidity, strong alkalinity, humidity, and more. Consequently, it is imperative to advance the development of LC-HEACs tailored to various application settings. This should be coupled with tribological assessments performed under simulated operational conditions that align with these diverse environments. Such efforts serve the dual purpose of expanding the potential applications of LC-HEACs and enhancing their overall application reliability.

(2) In numerous instances, both wear and corrosion phenomena manifest concurrently during machinery operation, with corrosion often exacerbating the wear experienced by the machinery. Consequently, it becomes essential to consider wear induced by corrosion when investigating the wear resistance of LC-HEACs. However, there is a noticeable scarcity of literature addressing the impact of tribo-corrosion coupling on LC-HEACs.

(3) At present, the LC-HEACs material system is relatively simple, and a more complete material system should be developed in future research. This could involve the incorporation of functionally graded coatings, serving the purpose of mitigating internal stress, preventing cracks, and enhancing the metallurgical bonding between the coating and the substrate. Furthermore, the inclusion of self-lubricating coatings with inherent self-lubricating properties holds promise. Given the escalating global energy crisis, the imperative of lightweight design cannot be overstated. Subsequently, it is advisable that forthcoming research efforts concentrate on the development of lighter HEAs material systems. Additionally, cost-effectiveness and considerations of industrial viability underscore the importance of designing HEAs material systems with economic feasibility in mind.

(4) The LC process parameters play a pivotal role in determining the quality of coatings produced. Nonetheless, the comprehensive understanding of the impact of these parameters on the wear resistance of coatings remains incomplete. This includes factors such as laser wavelength, power density (defined as the ratio of laser power to the laser spot area), overlap rate, and the technique employed for multi-layer cladding. Therefore, future research should focus on refining the investigation of how process parameters affect LC-HEACs and delve into the detailed mechanisms underlying their influence.

(5) The properties of the cladding layer in the laser cladding process are influenced by various physical fields, including the thermal field, magnetic field, and force field. These physical fields have a direct impact on the melting, crystallization, and cooling processes of the cladding layer, as well as the interface bonding and stress state between the cladding layer and the substrate. While current research has explored the influence of individual physical fields on cladding layer quality, the investigation into the effects of multiple physical fields remains relatively limited. Therefore, future research endeavors should focus on enhancing the simulation and experimental analysis of the coupling of multiple physical fields. This comprehensive exploration should delve into how these fields impact the physical and chemical reactions, microstructure evolution, and overall properties during the laser cladding process. Such investigations will offer valuable theoretical insights and practical guidance for optimizing laser cladding procedures and enhancing the cladding layer's properties.

## Declaration of competing interest

The authors declare that they have no conflicts of interest.

## Acknowledgments

The project was supported by the Guangdong Province Natural Science Foundation (2023A1515011558), the Ministry of Education Chunhui Plan Project (HZKY20220434), the State Key Laboratory of Solid Lubrication Fund (LSL-2204), the Science Fund of Key Laboratory for Precision and Non-Traditional Machining Technology of Ministry of Education (B202101), and the Open Project of Henan Key Laboratory of Intelligent Manufacturing of Mechanical Equipment, Zhengzhou University of Light Industry (No.IM202301). We are also grateful for the support from the Research Committee of The Hong Kong Polytechnic University (PolyU) (Project code: CD4F), PolyU Research and Innovation Office (Project code: BBR5), and the funding support for the State Key Laboratories in Hong Kong from the Innovation and Technology Commission of the Government of the Hong Kong Special Administrative Region, China. Thanks to Northeastern University Professor Zhao Ji for his useful comments and suggestions on this manuscript.

## References

[1] Wang J, Zhuang W, Liang W, et al. Inorganic nanomaterial lubricant additives for base fluids, to improve tribological performance: recent developments. Friction 2022;10(5):645–76.
[2] Luo J. New technologies that affect the development of manufacturing. Market Regulation Res China 2020;(10):12–4.
[3] Meng Y, Xu J, Jin Z, et al. A review of recent advances in tribology. Friction 2020;8(2):221–300.
[4] Pan S, Jin K, Wang T, et al. Metal matrix nanocomposites in tribology: manufacturing, performance, and mechanisms. Friction 2022;10(10):1596–634.
[5] Yin S, Li W, Song B, et al. Deposition of FeCoNiCrMn high entropy alloy (HEA) coating via cold spraying. J Mater Sci Technol 2019;35(6):1003–7.
[6] Song XT, Shi XH, Xia ZH, et al. Effects of Ni-P coating on mechanical properties of $Al_{0.3}$CoCrFeNi high-entropy alloys. Mater Sci Eng A 2019;752:152–9.
[7] Koshuro V, Fomina M, Fomin A. High-hardness carbide coatings and their production on X82WMoCrV6-5-4 steel using induction physical vapor deposition. Compos Struct 2022;281:115045.
[8] Schalk N, Tkadletz M, Mitterer C. Hard coatings for cutting applications: physical vs. chemical vapor deposition and future challenges for the coatings community. Surf Coating Technol 2022;429:127949.
[9] Larhlimi H, Ghailane A, Makha M, et al. Magnetron sputtered titanium carbide-based coatings: a review of science and technology. Vacuum 2022;197:110853.
[10] John M, Kalvala PR, Misra M, et al. Peening techniques for surface modification: processes, properties, and applications. Materials 2021;14(14):3841.
[11] Kaseem M, Fatimah S, Nashrah N, et al. Recent progress in surface modification of metals coated by plasma electrolytic oxidation: principle, structure, and performance. Prog Mater Sci 2021;117:100735.
[12] Jiang PF, Zhang CH, Wu CL, et al. Microstructure and properties of $CeO_2$-modified FeCoCrAlNiTi high-entropy alloy coatings by laser surface alloying. J Mater Eng Perform 2020;29(2):1346–55.
[13] Zhao Y, Zhang T, Chen L, et al. Microstructure and mechanical properties of Ti-C-TiN-reinforced Ni204-based laser-cladding composite coating. Ceram Int 2021;47(5):5918–28.
[14] Ye YF, Wang Q, Lu J, et al. High-entropy alloy: challenges and prospects. Mater Today 2016;19(6):349–62.
[15] Ren J, Zhang Y, Zhao D, et al. Strong yet ductile nanolamellar high-entropy alloys by additive manufacturing. Nature 2022;608(7921):62–8.
[16] Zhang Y, Zuo TT, Tang Z, et al. Microstructures and properties of high-entropy alloys. Prog Mater Sci 2014;61:1–93.
[17] Li K, Chen W. Recent progress in high-entropy alloys for catalysts: synthesis, applications, and prospects. Mater Today Energy 2021;20:100638.
[18] Yeh JW, Chen SK, Lin SJ, et al. Nanostructured high-entropy alloys with multiple principal elements: novel alloy design concepts and outcomes. Adv Eng Mater 2004;6(5):299–303.
[19] Miracle DB, Senkov ON. A critical review of high entropy alloys and related concepts. Acta Mater 2017;122:448–511.
[20] Ranganathan S. Alloyed pleasures: multimetallic cocktails. Curr Sci 2003;85(10):1404–6.

[21] Liu X, Fan J, Pu J, et al. Insight into the high-temperature tribological mechanism of VAlTiCrW high entropy alloy film: $AlV_3O_9$ from tribochemistry. Friction 2023;11(7):1165–76.
[22] Ren Y, Jia Q, DU Y, et al. A wear-resistant metastable CoCrNiCu high-entropy alloy with modulated surface and subsurface structures. Friction 2022;10(10):1722–38.
[23] Takeuchi A, Amiya K, Wada T, et al. High-entropy alloys with a hexagonal close-packed structure designed by equi-atomic alloy strategy and binary phase diagrams. JOM 2014;66(10):1984–92.
[24] Zhang F, Wu Y, Lou H, et al. Polymorphism in a high-entropy alloy. Nat Commun 2017;8(1):15687.
[25] Tong C, Chen Y, Chen S, et al. Microstructure characterization of $Al_x$CoCrCuFeNi high-entropy alloy system with multiprincipal elements. Metall Mater Trans A 2005;36(4):881–93.
[26] Senkov ON, Senkova SV, Dimiduk DM, et al. Oxidation behavior of a refractory $NbCrMo_{0.5}Ta_{0.5}TiZr$ alloy. J Mater Sci 2012;47(18):6522–34.
[27] Yeh J, Chang S, Hong Y, et al. Anomalous decrease in X-ray diffraction intensities of Cu-Ni-Al-Co-Cr-Fe-Si alloy systems with multi-principal elements. Mater Chem Phys 2007;103(1):41–6.
[28] Wang Y, Wang Y. High-entropy alloys in catalyses and supercapacitors: progress, prospects. Nano Energy 2022;104:107958.
[29] Archard JF. Contact and rubbing of flat surfaces. J Appl Phys 1953;24(8):981–8.
[30] Torres H, Caykara T, Hardell J, et al. Tribological performance of iron- and nickel-base self-lubricating claddings containing metal sulfides at high temperature[J]. 2022. Friction.
[31] Zhu L, Xue P, Lan Q, et al. Recent research and development status of laser cladding: a review. Opt Laser Technol 2021;138:106915.
[32] Chen L, Zhao Y, Song B, et al. Modeling and simulation of 3D geometry prediction and dynamic solidification behavior of Fe-based coatings by laser cladding. Opt Laser Technol 2021;139:107009.
[33] Chen L, Yu T, Xu P, et al. In-situ NbC reinforced Fe-based coating by laser cladding: simulation and experiment. Surf Coating Technol 2021;412:127027.
[34] Chen L, Zhao Y, Chen X, et al. Repair of spline shaft by laser-cladding coarse TiC reinforced Ni-based coating: process, microstructure and properties. Ceram Int 2021;47(21):30113–28.
[35] Liu Y, Ding Y, Yang L, et al. Research and progress of laser cladding on engineering alloys: a review. J Manuf Process 2021;66:341–63.
[36] Arif ZU, Khalid MY, Ur Rehman E, et al. A review on laser cladding of high-entropy alloys, their recent trends and potential applications. J Manuf Process 2021;68:225–73.
[37] Huang C, Zhang Y, Rui V, et al. Dry sliding wear behavior of laser clad TiVCrAlSi high entropy alloy coatings on Ti-6Al-4V substrate. Mater Des 2012;41:338–43.
[38] Wu W, Jiang L, Jiang H, et al. Phase evolution and properties of $Al_2$CrFeNiMo$_x$ high-entropy alloys coatings by laser cladding. J Therm Spray Technol 2015;24(7):1333–40.
[39] He B, Zhang N, Lin D, et al. The phase evolution and property of FeCoCrNiAlTi$_x$ high-entropy alloying coatings on Q253 via laser cladding. [J]. Coatings 2017;7(10):157.
[40] Lin D, Zhang N, He B, et al. Tribological properties of FeCoCrNiAlB$_x$ high-entropy alloys coating prepared by laser cladding. J Iron Steel Res Int 2017;24(2):184–9.
[41] Shu F, Yang B, Dong S, et al. Effects of Fe-to-Co ratio on microstructure and mechanical properties of laser cladded FeCoCrBNiSi high-entropy alloy coatings. Appl Surf Sci 2018;450:538–44.
[42] Liu H, Gao Q, Dai J, et al. Microstructure and high-temperature wear behavior of CoCrFeNiW$_x$ high-entropy alloy coatings fabricated by laser cladding. Tribol Int 2022;172:107574.
[43] Huang Y, Hu Y, Zhang M, et al. On the enhanced wear resistance of laser-clad CoCrCuFeNiTi$_x$ high-entropy alloy coatings at elevated temperature. Tribol Int 2022;174:107767.
[44] Yang J, Yan X, Wang C, et al. High-pressure wear behavior of laser clad MoNiTaTiV high-entropy alloy coating sliding against QBe2.0 beryllium bronze under dry and oil-lubricated conditions. Surf Coating Technol 2022;446:128757.
[45] Liu SS, Zhao GL, Wang XH, et al. Design and characterization of AlNbMoTaCu$_x$ high entropy alloys laser cladding coatings. Surf Coating Technol 2022;447:128832.
[46] Hui J, Han K, Li D, et al. Microstructure and mechanical properties investigation of the CoCrFeNiNb$_x$ high entropy alloy coatings. Crystals 2018;8(11):409.
[47] Qiu-Yi T, Xiu-Lin J, Jun D. Research on preparation of high-entropy composite coating reinforced by endogenous alumina particles and its anti-friction performance. Surf Technol 2021;50(11):218–25.
[48] Huang K, Chen L, Lin X, et al. Wear and corrosion resistance of $Al_{0.5}$CoCrCuFeNi high-entropy alloy coating deposited on AZ91D magnesium alloy by laser cladding. Entropy 2018;20(12):915.
[49] Guo YX, Liu QB, Zhou F. Microstructure and properties of $Fe_5Cr_5$SiTiCoNbMoW coating by laser cladding. Surf Eng 2018;34(4):283–8.
[50] Jiang H, Han K, Li D, et al. Synthesis and characterization of AlCoCrFeNiNb$_x$ high-entropy alloy coatings by laser cladding. Crystals 2019;9(1):56.
[51] Liang H, Yao H, Qiao D, et al. Microstructures and wear resistance of AlCrFeNi$_2$W$_{0.2}$Nb$_x$ high-entropy alloy coatings prepared by laser cladding. J Therm Spray Technol 2019;28(6):1318–29.
[52] Liu H, Liu J, Chen P, et al. Microstructure and properties of AlCoCrFeNiTi high-entropy alloy coating on AISI1045 steel fabricated by laser cladding. J Mater Eng Perform 2019;28(3):1544–52.
[53] Zhang Y, Han T, Xiao M, et al. Effect of Nb content on microstructure and properties of laser cladding FeNiCoCrTi$_{0.5}$Nb$_x$ high-entropy alloy coating. [J]. Optik 2019;198:163316.
[54] Cui Y, Shen J, Manladan SM, et al. Wear resistance of FeCoCrNiMnAl$_x$ high-entropy alloy coatings at high temperature. Appl Surf Sci 2020;512:145736.
[55] Xu Y, Li Z, Liu J, et al. Microstructure evolution and properties of laser cladding CoCrFeNiTiAl$_x$ high-entropy alloy coatings. J]. Coatings 2020;10(4):373.
[56] Li Y, Liang H, Nie Q, et al. Microstructures and wear resistance of CoCrFeNi$_2$V$_{0.5}$Ti$_x$ high-entropy alloy coatings prepared by laser cladding. Crystals 2020;10(5):352.
[57] Zhang GJ, Tian QW, Yin KX, et al. Effect of Fe on microstructure and properties of AlCoCrFe$_x$Ni (x=1.5, 2.5) high entropy alloy coatings prepared by laser cladding [J]. Intermetallics 2020;119:106722.
[58] Zhang G, Liu H, Tian X, et al. Microstructure and properties of AlCoCrFeNiSi high-entropy alloy coating on AISI 304 stainless steel by laser cladding. J Mater Eng Perform 2020;29(1):278–88.
[59] Cheng J, Sun B, Ge Y, et al. Effect of B/Si ratio on structure and properties of high-entropy glassy $Fe_{25}Co_{25}Ni_{25}(B_xSi_{1-x})_{25}$ coating prepared by laser cladding. Surf Coating Technol 2020;402:126320.
[60] Sun Z, Zhang M, Wang G, et al. Wear and corrosion resistance analysis of FeCoNiTiAl$_x$ high-entropy alloy coatings prepared by laser cladding. [J]. Coatings 2021;11(2):155.
[61] Zhao P, Li J, Zhang Y, et al. Wear and high-temperature oxidation resistances of AlNbTaZr$_x$ high-entropy alloys coatings fabricated on Ti6Al4V by laser cladding. J Alloys Compd 2021;862:158405.
[62] Liu H, Li X, Liu J, et al. Microstructural evolution and properties of dual-layer CoCrFeMnTi$_{0.2}$ high-entropy alloy coating fabricated by laser cladding[J. Opt Laser Technol 2021;134:106646.
[63] Wen X, Cui X, Jin G, et al. In-situ synthesis of nano-lamellar $Ni_{1.5}CrCoFe_{0.5}Mo_{0.1}Nb_x$ eutectic high-entropy alloy coatings by laser cladding: alloy design and microstructure evolution. Surf Coating Technol 2021;405:126728.
[64] Yang Y, Ren Y, Tian Y, et al. Microstructure and tribological behaviors of FeCoCrNiMoSi$_x$ high-entropy alloy coatings prepared by laser cladding. Surf Coating Technol 2022;432:128009.
[65] Li X, Feng Y, Wang X, et al. Microstructures and properties of AlCrFeNiMn$_x$ high-entropy alloy coatings fabricated by laser cladding on a copper substrate. J Alloys Compd 2022;926:166778.
[66] Ostovari Moghaddam A, Samodurova MN, Pashkeev K, et al. A novel intermediate temperature self-lubricating CoCrCu$_{1-x}$FeNi$_x$ high entropy alloy fabricated by direct laser cladding. Tribol Int 2021;156:106857.
[67] Shi FK, Zhang QK, Xu C, et al. In-situ synthesis of NiCoCrMnFe high entropy alloy coating by laser cladding. Opt Laser Technol 2022;151:108020.
[68] Wu H, Zhang S, Wang ZY, et al. New studies on wear and corrosion behavior of laser cladding FeNiCoCrMo$_x$ high entropy alloy coating: the role of Mo. Int J Refract Metals Hard Mater 2022;102:105721.
[69] Gu Z, XI S, Sun C. Microstructure and properties of laser cladding and $CoCr_{2.5}FeNi_2Ti_x$ high-entropy alloy composite coatings. J Alloys Compd 2020;819:152986.
[70] Qiu XW, Zhang YP, Liu CG. Effect of Ti content on structure and properties of $Al_2$CrFeNiCoCuTi$_x$ high-entropy alloy coatings. J Alloys Compd 2014;585:282–6.
[71] Zhang Y, Han T, Xiao M, et al. Effect of iron content on microstructure and properties of Fe$_x$Ni$_2$Co$_2$CrTiNb high-entropy alloy coating. Optik 2020;204:164168.
[72] Gu Z, X S, Mao P, et al. Microstructure and wear behavior of mechanically alloyed powder $Al_xMo_{0.5}$NbFeTiMn$_2$ high entropy alloy coating formed by laser cladding. Surf Coating Technol 2020;401:126244.
[73] Li Y, Shi Y, Olugbade E. Microstructure, mechanical, and corrosion resistance properties of $Al_{0.8}$CrFeCoNiCu$_x$ high-entropy alloy coatings on aluminum by laser cladding. Mater Res Express 2020;7(2):26504.
[74] Qiu X, Liu C. Microstructure and properties of $Al_2$CrFeCoCuTiNi$_x$ high-entropy alloys prepared by laser cladding. J Alloys Compd 2013;553:216–20.
[75] Lin D, Zhang N, He B, et al. Structural evolution and performance changes in FeCoCrNiAlNb$_x$ high-entropy alloy coatings cladded by laser. J Therm Spray Technol 2017;26(8):2005–12.
[76] Fu Y, Huang C, DU C, et al. Evolution in microstructure, wear, corrosion, and tribocorrosion behavior of Mo-containing high-entropy alloy coatings fabricated by laser cladding. Corrosion Sci 2021;191:109727.
[77] Liu H, Sun S, Zhang T, et al. Effect of Si addition on microstructure and wear behavior of AlCoCrFeNi high-entropy alloy coatings prepared by laser cladding. Surf Coating Technol 2021;405:126522.
[78] Liu D, Zhao J, Li Y, et al. Effects of boron content on microstructure and wear properties of FeCoCrNiB$_x$ high-entropy alloy coating by laser cladding. Appl Sci 2019;10(1):49.
[79] Aguilar-Hurtado JY, Vargas-Uscategui A, Paredes-Gil K, et al. Boron addition in a non-equiatomic $Fe_{50}Mn_{30}Co_{10}Cr_{10}$ alloy manufactured by laser cladding: microstructure and wear abrasive resistance. Appl Surf Sci 2020;515:146084.
[80] Jiang L, Wu W, Cao Z, et al. Microstructure evolution and wear behavior of the laser cladded CoFeNi$_2$V$_{0.5}$Nb$_{0.75}$ and CoFeNi$_2$V$_{0.5}$Nb high-entropy alloy coatings. J Therm Spray Technol 2016;25(4):806–14.
[81] Guo Y, Liu Q. MoFeCrTiWAlNb refractory high-entropy alloy coating fabricated by rectangular-spot laser cladding. Intermetallics 2018;102:78–87.
[82] Wang H, Zhang W, Peng Y, et al. Microstructures and wear resistance of FeCoCrNi-Mo high entropy alloy/diamond composite coatings by high speed laser cladding. [J]. Coatings 2020;10(3):300.
[83] Malatji N, Popoola API, Lengopeng T, et al. Tribological and corrosion properties of laser additive manufactured AlCrFeNiCu high entropy alloy. Mater Today Proc 2020;28:944–8.

[84] Wei X, Zhang P, Yu Z, et al. Effect of phase transformation on mechanical properties of $Al_{16.80}Co_{20.74}Cr_{20.49}Fe_{21.28}Ni_{20.70}$ high entropy alloy coatings processed by laser cladding. J Alloys Compd 2021;862:158563.

[85] Shu F, Zhang B, Liu T, et al. Effects of laser power on microstructure and properties of laser cladded CoCrBFeNiSi high-entropy alloy amorphous coatings. Surf Coating Technol 2019;358:667–75.

[86] Peng YB, Zhang W, Li TC, et al. Microstructures and mechanical properties of FeCoCrNi high entropy alloy/WC reinforcing particles composite coatings prepared by laser cladding and plasma cladding. Int J Refract Metals Hard Mater 2019;84:105044.

[87] Ma Q, Lu B, Zhang Y, et al. Crack-free 60 wt% WC reinforced FeCoNiCr high-entropy alloy composite coating fabricated by laser cladding. Mater Lett 2022;324:132667.

[88] Li X, Feng Y, Liu B, et al. Influence of NbC particles on microstructure and mechanical properties of AlCoCrFeNi high-entropy alloy coatings prepared by laser cladding. J Alloys Compd 2019;788:485–94.

[89] Xu Y, Wang G, Song Q, et al. Microstructure, mechanical properties, and corrosion resistance of SiC reinforced $Al_xCoCrFeNiTi_{1-x}$ high-entropy alloy coatings prepared by laser cladding. Surf Coating Technol 2022;437:128349.

[90] Yuanbin Z, Ping Z, Haomin L, et al. The effect of Ti and $B_4C$ on the microstructure and properties of the laser clad FeCoCrNiMn based high entropy alloy coating. Surf Coating Technol 2022;441:128499.

[91] Jiang J, Li R, Yuan T, et al. Microstructural evolution and wear performance of the high-entropy FeMnCoCr alloy/TiC/$CaF_2$ self-lubricating composite coatings on copper prepared by laser cladding for continuous casting mold. J Mater Res 2019;34(10):1714–25.

[92] Cai Y, Ao S, Manladan SM, et al. Evolution mechanisms of TiC ceramic particles in FeCoCrNiAl high-entropy alloy laser cladding layers. Mater Res Express 2019;6(10):1062d–5d.

[93] Zhao M, Wu T, Liu D, et al. Effect of carbon fiber on microstructure evolution and surface properties of FeCoCrNiCu high-entropy alloy coatings. Mater Corros 2020;71(3):430–9.

[94] Shang X, Bo S, Guo Y, et al. ZrC reinforced refractory-high-entropy-alloy coatings: compositional design, synthesis, interstitials, and microstructure evolution effects on wear, corrosion and oxidation behaviors. Appl Surf Sci 2021;564:150466.

[95] Jiang D, Cui H, Chen H, et al. Wear and corrosion properties of $B_4C$-added CoCrNiMo high-entropy alloy coatings with in-situ coherent ceramic. Mater Des 2021;210:110068.

[96] Wang L, Gao Z, Wu M, et al. Influence of specific energy on microstructure and properties of laser cladded FeCoCrNi high entropy alloy. [J]. Metals 2020;10(1464):1464.

[97] Tamanna N, Crouch R, Naher S. Progress in numerical simulation of the laser cladding process. [J]. Optics and Lasers in Engineering 2019;122:151–63.

[98] Cai Y, Zhu L, Cui Y, et al. Fracture and wear mechanisms of FeMnCrNiCo+x(TiC) composite high-entropy alloy cladding layers. Appl Surf Sci 2021;543:148794.

[99] Lu K, Zhu J, Guo D, et al. Microstructures, corrosion resistance and wear resistance of high-entropy alloys coatings with various compositions prepared by laser cladding: a review. [J]. Coatings 2022;12(7):1023.

[100] Zhang Y, Han T, Xiao M, et al. Preparation of diamond reinforced $NiCoCrTi_{0.5}Nb_{0.5}$ high-entropy alloy coating by laser cladding: microstructure and wear behavior. J Therm Spray Technol 2020;29(7):1827–37.

[101] Zhang Y, Han T, Xiao M, et al. Tribological behavior of diamond reinforced $FeNiCoCrTi_{0.5}$ carbonized high-entropy alloy coating. Surf Coating Technol 2020;401:126233.

[102] Bu F, Li C, Shen C, et al. Microstructures and wear resistance of diamond-reinforced $FeCoCrNiAl_{0.5}Ti_{0.5}Si_{0.2}$-carbonized high-entropy alloy coatings by laser cladding. Trans Indian Inst Met 2022;75(8):1967–78.

[103] Guo Y, Shang X, Liu Q. Microstructure and properties of in-situ TiN reinforced laser cladding $CoCr_2FeNiTi_x$ high-entropy alloy composite coatings. Surf Coating Technol 2018;344:353–8.

[104] Guo Y, Li C, Zeng M, et al. In-situ TiC reinforced $CoCrCuFeNiSi_{0.2}$ high-entropy alloy coatings designed for enhanced wear performance by laser cladding. Mater Chem Phys 2020;242:122522.

[105] Yan G, Zheng M, Ye Z, et al. In-situ Ti(C, N) reinforced AlCoCrFeNiSi-based high entropy alloy coating with functional gradient double-layer structure fabricated by laser cladding. J Alloys Compd 2021;886:161252.

[106] Liang G, Jin G, Cui X, et al. Synthesis and characterization of directional array TiN-reinforced AlCoCrCuNiTi high-entropy alloy coating by magnetic-field-assisted laser cladding. J Mater Eng Perform 2021;30(5):3568–76.

[107] Liang G, Jin G, Cui X, et al. The directional array TiN-reinforced AlCoCrFeNiTi high-entropy alloy synthesized in situ via magnetic field-assisted laser cladding. Appl Surf Sci 2022;572:151407.

[108] Li Y, Wang K, Fu H, et al. Microstructure and wear resistance of in-situ TiC reinforced AlCoCrFeNi-based coatings by laser cladding. Appl Surf Sci 2022;585:152703.

[109] Liu H, Liu J, Chen P, et al. Microstructure and high temperature wear behaviour of in-situ TiC reinforced AlCoCrFeNi-based high-entropy alloy composite coatings fabricated by laser cladding. Opt Laser Technol 2019;118:140–50.

[110] Liu SS, Zhang M, Zhao GL, et al. Microstructure and properties of ceramic particle reinforced FeCoNiCrMnTi high entropy alloy laser cladding coating. Intermetallics 2022;140:107402.

[111] Mishra D, Maurya R, Verma V, et al. Understanding the influence of graphene-based lubricant/coating during fretting wear of zircaloy. Wear 2023:204527. 512-513.

[112] Pan S, Saso T, Yu N, et al. New study on tribological performance of AA7075-TiB2 nanocomposites. Tribol Int 2020;152:106565.

[113] Musharavati F, Jaber F, Nasor M, et al. Micromechanical properties of hydroxyapatite nanocomposites reinforced with CNTs and $ZrO_2$. Ceram Int 2023;49(5):7466–75.

[114] Huang Y, Wu D, Zhao D, et al. Investigation of melt-growth alumina/aluminum titanate composite ceramics prepared by directed energy deposition. Int J Extrem Manuf 2021;3(3):35101.

[115] Torres H, Rodríguez Ripoll M, Prakash B. Tribological behaviour of self-lubricating materials at high temperatures. Int Mater Rev 2018;63(5):309–40.

[116] Geng Y, Chen J, Tan H, et al. Tribological performances of CoCrFeNiAl high entropy alloy matrix solid-lubricating composites over a wide temperature range. Tribol Int 2021;157:106912.

[117] Das AK. Effect of rare earth oxide additive in coating deposited by laser cladding: a review. Mater Today Proc 2022;52:1558–64.

[118] Gu Z, Mao P, Gou Y, et al. Microstructure and properties of $MgMoNbFeTi_2Y_x$ high entropy alloy coatings by laser cladding. Surf Coating Technol 2020;402:126303.

[119] Liu J, Guan Y, Xia X, et al. Laser cladding of $Al_{0.5}CoCrCuFeNiSi$ high entropy alloy coating without and with yttria addition on H13 steel. Crystals 2020;10(4):320.

[120] Shu F, Tian Y, Jiang S, et al. Effect of rare earth oxide $CeO_2$ on microstructure and surface properties of laser cladded CoFeCrNiSiB high-entropy alloy coatings. Mater Res Express 2019;6(10):106517.

[121] Cheng J, Sun B, Ge Y, et al. Nb doping in laser-cladded $Fe_{25}Co_{25}Ni_{25}(B_{0.7}Si_{0.3})_{25}$ high entropy alloy coatings: microstructure evolution and wear behavior. Surf Coating Technol 2020;402:126321.

[122] Shu FY, Wu L, Zhao HY, et al. Microstructure and high-temperature wear mechanism of laser cladded CoCrBFeNiSi high-entropy alloy amorphous coating. Mater Lett 2018;211:235–8.

[123] Zhao Y, Wu M, Jiang P, et al. Microstructure of WTaNbMo refractory high entropy alloy coating fabricated by dynamic magnetic field assisted laser cladding process. J Mater Res Technol 2022;20:1908–11.

[124] Zhao Y, Wu M, Hou J, et al. Microstructure and high temperature properties of laser cladded WTaNbMo refractory high entropy alloy coating assisted with ultrasound vibration. J Alloys Compd 2022;920:165888.

[125] Wen X, Cui X, Jin G, et al. Design and characterization of $FeCrCoAlMn_{0.5}Mo_{0.1}$ high-entropy alloy coating by ultrasonic assisted laser cladding. J Alloys Compd 2020;835:155449.

[126] Cui G, Han B, Yang Y, et al. Sulfurizing of $CoCrFeNiSi_{0.4}$ and CoCrFeMoNi high entropy alloys fabricated by laser cladding. Surf Coating Technol 2020;381:125182.

[127] Cai Z, Cui X, Liu Z, et al. Microstructure and wear resistance of laser cladded Ni-Cr-Co-Ti-V high-entropy alloy coating after laser remelting processing. Opt Laser Technol 2018;99:276–81.

[128] Cui Z, Mi Y, Qiu D, et al. Microstructure and mechanical properties of additively manufactured CrMnFeCoNi high-entropy alloys after ultrasonic surface rolling process. J Alloys Compd 2021;887:161393.

[129] Guo Y, Wang H, Liu Q. Microstructure evolution and strengthening mechanism of laser-cladding $MoFe_xCrTiWAlNb_y$ refractory high-entropy alloy coatings. J Alloys Compd 2020;834:155147.

[130] Liu H, Liu J, Li X, et al. Effect of heat treatment on phase stability and wear behavior of laser clad $AlCoCrFeNiTi_{0.8}$ high-entropy alloy coatings. Surf Coating Technol 2020;392:125758.

[131] Kuang S, Zhou F, Zheng S, et al. Annealing-induced microstructure and properties evolution of refractory $MoFeCrTiWAlNb_3$ eutectic high-entropy alloy coating by laser cladding. Intermetallics 2021;129:107039.

[132] Gao N, Wang CT, Wood RJK, et al. Tribological properties of ultrafine-grained materials processed by severe plastic deformation. J Mater Sci 2012;47(12):4779–97.

[133] Rupert TJ, Schuh CA. Sliding wear of nanocrystalline Ni-W: structural evolution and the apparent breakdown of archard scaling. Acta Mater 2010;58(12):4137–48.

[134] Liu C, Li Z, Lu W, et al. Reactive wear protection through strong and deformable oxide nanocomposite surfaces. Nat Commun 2021;12(1):5518.

[135] Yue TM, Huang KJ. Laser cladding of $Cu_{0.5}NiAlCoCrFeSi$ high entropy alloy on AZ91D magnesium substrates for improving wear and corrosion resistance. World Journal of Engineering 2012;9(2):119–24.

[136] Wang H, Liu Q, Guo Y, et al. $MoFe_{1.5}CrTiWAlNb_x$ refractory high-entropy alloy coating fabricated by laser cladding. [J]. Intermetallics 2019;115:106613.

[137] Zeng X, Liu Z, Wu G, et al. Microstructure and high-temperature properties of laser cladded $AlCoCrFeNiTi_{0.5}$ high-entropy coating on Ti 6Al-4V alloy. Surf Coating Technol 2021;418:127243.

[138] Huang Y, Wang Z, Xu Z, et al. Microstructure and properties of TiNbZrMo high entropy alloy coating. Mater Lett 2021;285:129004.

[139] Zhang Y, Han T, Xiao M, et al. Microstructure and properties of laser-clad $FeNiCoCrTi_{0.5}Nb_{0.5}$ high-entropy alloy coating. Mater Sci Technol 2020;36(7):811–8.

[140] Liu X, Lei W, Li J, et al. Laser cladding of high-entropy alloy on H13 steel. Rare Met 2014;33(6):727–30.

[141] Gu Z, Peng W, Guo W, et al. Design and characterization on microstructure evolution and properties of laser-cladding $Ni_{1.5}CrFeTi_2B_{0.5}Mo_x$ high-entropy alloy coatings[J]. Surf Coating Technol 2021;408:126793.

[142] Liang H, Qiao D, Miao J, et al. Anomalous microstructure and tribological evaluation of $AlCrFeNiW_{0.2}Ti_{0.5}$ high-entropy alloy coating manufactured by laser cladding in seawater[J]. J Mater Sci Technol 2021;85:224–34.

[143] Qiu X. Microstructure and mechanical properties of CoCrFeNiMo high-entropy alloy coatings[J]. J Mater Res Technol 2020;9(3):5127–33.

[144] Shu F, Wang B, Zhao H, et al. Effects of line energy on microstructure and mechanical properties of CoCrFeNiBSi high-entropy alloy laser cladding coatings [J]. J Therm Spray Technol 2020;29(4):789–97.
[145] Lan H, Liu Q. Design of [Al-$(FeCoNi)_{12}$]$Al_xCr_{3-x}$ HEAs based on cluster-plus-glue-atom model and its coating fabricated by laser cladding[J]. Intermetallics 2020; 126:106941.
[146] Li Y, Shi Y. Microstructure and wear resistance of the laser-cladded $Al_{0.8}CrFeCoNiCu_{0.5}B_x$ high-entropy alloy coating on aluminum[J]. Mater Res Express 2020;7(2):26517.
[147] Li Y, Shi Y. Phase assemblage and wear resistance of laser-cladding $Al_{0.8}FeCoNiCrCu_{0.5}Si_x$ high-entropy alloys on aluminum[J]. Mater Res Express 2020;7(8):86504.
[148] Jin G, Cai Z, Guan Y, et al. High temperature wear performance of laser-cladded FeNiCoAlCu high-entropy alloy coating[J]. Appl Surf Sci 2018;445:113–22.
[149] Gunen A, Lindner T, Karakas MS, et al. Effect of the boriding environment on the wear response of laser-clad AlCoCrFeNi high entropy alloy coatings[J]. Surf Coating Technol 2022;447:128830.
[150] Zhang HX, Dai JJ, Sun CX, et al. Microstructure and wear resistance of TiAlNiSiV high-entropy laser cladding coating on Ti-6Al-4V[J]. J Mater Process Technol 2020;282:116671.
[151] Liang H, Miao J, Gao B, et al. Microstructure and tribological properties of $AlCrFe_2Ni_2W_{0.2}Mo_{0.75}$ high-entropy alloy coating prepared by laser cladding in seawater, NaCl solution and deionized water. Surf Coating Technol 2020;400: 126214.
[152] Deng C, Wang C, Chai L, et al. Mechanical and chemical properties of $CoCrFeNiMo_{0.2}$ high entropy alloy coating fabricated on Ti6Al4V by laser cladding[J]. Intermetallics 2022;144:107504.
[153] Zhang M, Wang D, He L, et al. Microstructure and elevated temperature wear behavior of laser-cladded AlCrFeMnNi high-entropy alloy coating[J]. Opt Laser Technol 2022;149:107845.
[154] Cui Y, Shen J, Hu S, et al. Oxidation and wear mechanisms of $FeCoCrNiMnAl_x$ cladding layers at high-temperature condition[J]. Coatings 2020;10(11):1136.